A

PROPOSAL

FOR

ICRF HEATING OF ALCATOR-C

H. Takahashi and R. R. Parker

December 1979, PFC/RR-80-8

Plasma Fusion Center
Massachusetts Institute of Technology
Cambridge, Mass. 01239

LIST OF CONTENTS

A PROPOSAL FOR ICRF HEATING OF ALCATOR-C

1. SUMMARY

This report contains the physics and engineering sections of a proposal submitted to the U. S. Department of Energy in December, 1979.

1.1 Objectives

We aim at achieving the following two principal objectives:

(1)to add at least 4 MW of radiofrequency (RF) power to the plasma in the ion cyclotron range of frequencies (ICRF).

(2)to delineate minimum requirements of the ICRF technique on the tokamak structure in time to make significant contributions to the design of the next generation of tokamaks.

Given both good heating efficiency and anticipated tokamak performance, the addition of 4 MW of RF power is expected to bring the plasma to the threshold of thermonuclear regimes. This will enable us to test the continued effectiveness of ICRF heating in these regimes.

1.2 Methods and Equipment

In order to achieve the first goal, as many antennae as necessary will be installed on the Alcator-C. An antenna design, capable of delivering an RF power of the order of 1 MW per antenna and compatible with the constraints imposed by the Alcator-C port structure, will be developed.

In order to achieve the second goal, we will attempt to define the minimum conditions necessary for a structure to function as an antenna and to determine to what degree ICRF antennae can be an integral part of the tokamak design.

The bulk of the RF amplifier equipment, suitable for heating hydrogen plasmas at moderate fields, helium-3 plasmas at high fields and deuterium plasmas at very high fields, is already at hand. However, a DC power supply capable of long pulse operations at a 10 MW level needs to be procured. Some new and spare amplifier tubes may also have to be purchased.

For experiments in deuterium plasma at moderate to high field modifications must be made to the existing RF amplifiers for lower frequency operations. Modified equipment will have long-range use in future tokamak heating.

2. INTRODUCTION

2.1 Current Status of ICRF Heating - A Historical Perspective

ICRF heating of a tokamak plasma makes use of one of the two branches of the cold plasma wave dispersion relation, variously called compressional Alfven waves, magnetoacoustic waves or simply, fast waves. It is distinct from the so-called ion cyclotron resonance heating (ICRH). ICRH makes use of the other branch of the dispersion relation called ion cyclotron waves, that experience the ion cyclotron resonance -- one of the principal resonances of the cold plasma waves. The success of this method in heating stellarator plasmas(1) made the term ICRH a generic term for all rf heating in the ion cyclotron range of frequencies. Physical processes that lead to plasma heating are, however, different for the two heating methods. The term, ICRF heating -- short for ion cyclotron range of frequencies heating -- was coined in the hope of making this distinction.

Experimentation with the fast waves in tokamak plasmas was initiated around 1970 by Russian researchers(2). Working at frequencies several times the ion cyclotron frequency of the major constituent ions, they observed oscillations of plasma-filled toroidal cavities that could be interpreted as excitation of the fast waves. They thought of exploiting high-Q oscillations and attendant high wave field strength to heat the plasma. The exact nature of the wave absorption mechanisms,

however, was not identified.

The first serious analysis of ICRF heating of tokamak plasmas was done in 1971 by Adam and Samain(3). The second harmonic cyclotron damping caused by the majority ion species and the fundamental cyclotron damping by the minority constituent were identified as the wave absorption mechanisms that could be utilized for plasma heating. Experiments were performed at rf power levels high enough to significantly affect the plasma temperature in the TM-1 tokamak(4) in 1973, and in the ST(5) and TO-1(6) tokamaks in 1974. A series of experiments, starting from the ST experiments and followed by ATC, TFR and PLT experiments, was aided by increasingly sophisticated means of tokamak diagnostics and computer data acquisition, and lead to the current state of the art that allows prediction of ICRF performance in future tokamaks to be made with an increasing degree of confidence. Some important results from this series of experiments are presented in the remaining part of this section.

The clearest evidence of fast wave excitation obtained to date was produced in the ST experiments(5). The upper part of Fig. 1 shows a tone plot of the experimentally observed antenna loading resistance as a function of the toroidal magnetic field strength (expressed in terms of the wave to ion cyclotron frequencies) and time (or equivalently, plasma density). Darker tone indicates high loading resistance caused by the occurrence of toroidal eigenmode resonances. The lower part of Fig. 1 shows

the corresponding predictions based upon the theory of fast wave propagation. Nearly complete agreement between the experimental observations and theoretical predictions leaves little doubt that the excited waves were indeed the fast waves.

Clear indications of heating effect were also observed in the ST experiments. The neccessity to match the ion cyclotron frequency to the existing generator frequency, however, forced tokamak operation in derated, low-current, low-density regimes. Heating at a moderate power and long pulse length was masked by the so-called "impurity heating". Experiments were therefore conducted with a very short (typically one millisecond or shorter), high-power rf pulse. Rise in temperature was registered by the charge exchange instruments in both the perpendicular and parallel directions, qualitatively confirming the existence of heating. The quantitative assessment of temperature rise, however, was probably overly optimistic, because evidence was found later that the measurements were significantly influenced by the presence of minority proton species in dominantly deuteron plasmas. Rapid rise (as well as fall) of the measured temperature was (again in hindsight) indicative of power absorption by a species with a small thermal capacity. The deuteron-on-proton relaxation time was much longer than the heating pulse length because of low plasma density. The so-called impurity heating might also have been only apparent temperature rise caused by an idiosyncracy of the charge exchange measurement.

Recognizing need for experimentation under better plasma conditions and at heating pulse lengths significantly longer than various relaxation times, experiments(7) were repeated in 1976 in the ATC device, whose operating characteristics were better matched to the rf generator. By this time improved diagnostic devices were available including a five-channel charge exchange analyzer (as opposed to the one-channel device used in ST) and a scanning monochrometer capable of obtaining time-resolved Doppler profiles of impurity lines. Measurements by these instruments together with neutron diagnostics made it possible to ascertain that substantial heating of the majority deuteron species was possible. Furthermore, it was possible for the first time to determine the radial temperature profile that showed heating of the central core of the plasma. The maximum temperature rise of 200 eV was observed at an rf power of 145 kW and at an on-axis plasma density of $2.2 \times 10^{19}/m^3$. This amounts to 1.4 eV/kW for the stated density, or 0.6 eV/kW/$10^{19}/m^3$ when normalized with respect to the central density.

Meanwhile a significant advance was made in the TFR(8) and ATC(9) experiments in understanding of the physics of ICRF heating. In these experiments the wave damping strength was found to be much stronger than theoretical predictions, and the position of the strongest damping was located asymmetrically with respect to the plasma center. This result was attributed to the influence of the two-ion hybrid resonance between the majority

deuteron and minority proton species. Analysis of wave damping due to mode conversion at the hybrid layer was first carried out by Swanson(10). Analyses by a number of other researchers followed(11)(12). To date three different wave damping mechanisms are identified: (1)minority species fundamental cyclotron damping, (2)majority species second harmonic cyclotron damping and (3)mode conversion damping at two-ion hybrid resonance. In addition, both the minority species and second harmonic damping may be enhanced due to the presence of the hybrid resonance in the proximity of the cyclotron resonance(13).

The trend toward better understanding of the ICRF physics and the unequivocal establishment of the efficacy of the method culminated in the recent experiments in the PLT device. The experimental efforts, focused on the minority heating, were aided by an impressive array of sophisticated tokamak diagnostics. These included a multi-channel, mass-analyzed charge exchange detector, time- and space-resolved scanning UV monochrometer, energy-resolved neutron counter and X-ray Doppler broadening spectroscopy, all for ion temperature measurements, a multi-channel Thomson scattering device, an electron cyclotron emmission detector and soft x-ray analyzer for electron temperature measurements, and a spatially resolved bolometric measurement system for power balance. Out of these multitudes of diagnostic results a consistent and convincing picture of the efficacy of ICRF heating emerged. In Fig. 2 radial variations of the ion temperature in PLT measured with and without an rf pulse

is shown. The measurements made by four independent diagnostic techniques are consistent with each other and clearly indicate a substantial heating of the central core of the plasma. Fig. 3 shows the measured temperature rise as a function of rf power for two cases, one with proton minority species and the other with helium-3 minority species, both in deuteron majority plasmas. Ion heating efficiencies of 40 % and 80 % are obtained for the proton and helium cases, respectively(14). Higher efficiency for the helium case was attributed to more effective slowing-down of helium ions by electron drag that results in smaller production of energetic particles. In Fig. 4 the distribution of high-energy proton tail observed in PLT(15) is compared to theoretical prediction based upon Stix's theory(16). Good agreement between the experiments and theory indicate that this theory may be used for predicting tail generation in future minority heating experiments. (Comparisons between experiments and Stix's theory made in PLT and also in TFR(17) are preceeded by one done in T-4(18)).

Recent experimental efforts in TFR are centered around two-ion hybrid heating. The top half of Fig. 5 shows the effect on the neutron counting rate of varying the proton-to-deuteron concentration ratio. Under the condition marked, a, in which the proton concentration is small and both the proton cyclotron and ion hybrid resonance layers are near the plasma center, a large neutron counting rate was obtained. This indicates the effectiveness of the minority heating (theoretically, the mode

conversion heating is predicted to be small when the minority concentration is very small). Under the conditiion marked, b, in which the proton concentration was sizable and the hybrid layer was moved toward the plasma edge while the cyclotron layer remained near the center, a very small counting rate was observed. Under the condition marked, c, the proton concentration remained same as the case, b, but the hybrid layer was positioned near the center and the cyclotron layer was pushed toward the plasma edge. A large neutron counting rate was again observed. The latter two cases showed that at higher proton concentrations it was the hybrid resonance that was responsible for heating (theoretically, the minority heating is predicted to be weak at high proton concentrations). In the lower half of Fig. 5 the observed temperature rise normalized by the rf power is plotted as a function of the two-ion hybrid resonance location. The proton cyclotron resonance layer position remained fixed near the plasma edge and the minority heating contributions were negligible in these experiments. These two sets of experiments showed clearly the efficacy of two-ion hybrid heating under the conditions in which it was theoretically expected to be effective, i.e., at high proton concentrations.

Preliminary reports from DIVA group(19) indicate that effective heating could also be obtained from pure second harmonic damping of the fast wave. This heating mechanism is, however, less thoroughly explored compared to the minority and two-ion hybrid heating, mainly because of slow heating rate under

the plasma conditions prevailing in the past tokamak experiments. However, the second harmonic heating rate, which is proportional to the product of the ion density and temperature, is expected to become increasingly important in hotter and denser plasmas.

Reflecting perhaps a heightened expectation that ICRF heating will play a major role in future reactor heating, many smaller installations entered into the ICRF research field, significantly broadening the ICRF research base. These new projects focused their attention on many of the physics questions left unanswered by the larger, more mission-oriented projects. These new projects include Macrotor(20), Caltech Tokamak(21), Texas Tech Tokamak(22), Alcator-A(23) and Erasmus(24). Increasingly more detailed information on antenna loading, wave damping and propagation began to emerge from these new endeavors.

The current status of ICRF heating can be summarized as follows:

(1)The efficacy of ICRF heating is unequivocally established for the plasma conditions prevailing in the existing tokamaks.

(2)The maximum rf power coupled to any tokamak is limited to about 500 kW and the highest achieved plasma temperature is well below thermonuclear regime.

(3)At least three different wave absorption mechanisms are identified -- the minority fundamental cyclotron, two-ion hybrid and majority second harmonic cyclotron damping --

depending upon the wave frequency, toroidal field strength and plasma composition, and the gross behavior of heating caused by these mechanisms are in agreement with theoretical expectations.

2.2 Why the Alcator-C Experiments?

Having demonstrated in recent years an important principle that high-field tokamaks are uniquely suited for producing very high density plasmas with good confinement, Alcator devices now face an important question: can plasmas in such devices be heated to thermonuclear temperatures by means of a suitable additional heating? On one hand, neutral beam heating -- a proven additional heating method for low density tokamak plasmas -- would have difficult problems of beam penetration into very high density Alcator-C plasma and of severely limited access to the plasma. On the other hand, the efficacy of ICRF heating is unequivocally established and there are many reasons to believe that high-density Alcator-C plasmas are uniquely suited for ICRF heating. The principal thrust of the proposed project is the use of ICRF heating as a means of bringing Alcator-C plasmas into thermonuclear regimes rather than studies of ICRF heating by itself, although many unanswered questions regarding the heating technique will be addressed in the course of the project.

The operating ranges of Alcator-C and other on-going ICRF projects are shown in Fig. 6 in order to put the relationship among these projects into perspective. The ordinate of the

figure is the rf generator frequency and the abscissa the toroidal magnetic field strength. Conditions of cyclotron and cyclotron harmonic resonances are shown by straight lines for various combinations of the harmonic number, n, nuclear charge, Z, and atomic number, A. Two-ion hybrid resonance occurs between the fundamental cyclotron resonances of the ion species involved. The ranges denoted as PLT-1 and PLT-2 correspond to the generator frequencies of 25 MHz and 45 MHz, respectively. The generator frequency for Alcator-C is adjustable over the range indicated in the figure. The three major ICRF heating experiments shown in the figure cover widely different regimes of field and frequency. Accordingly the plasma parameters are quite different. The table below lists some plasma parameters of the Alcator-C and PLT. We suppose that both the ion and electron temperatures reach 4 keV as a result of applying 4 MW of rf power. The plasma volume of PLT is eleven times greater than that of Alcator-C, but the density of the PLT plasma is a factor of 50 smaller than that of Alcator-C. On balance Alcator-C has four times the number of particles to be heated and four times greater internal energy (both electron and ion energy). The on-axis rf power density is again eleven times greater for Alcator-C than for PLT, but the power per particle is a factor of four smaller for Alcator-C than PLT. (The latter quantity, tabulated in units of keV/sec, multiplied by the energy confinement time gives the asymptotic temperature rise at 100 % heating efficiency.) The energy confinement time of Alcator-C entered in the table is a value expected from the so-called Alcator-A scaling law(see below).

The ξ-parameter will be discussed in a later section. Because of these widely different plasma parameters and rf power densities, different physics would govern ICRF heating of these devices. In particular, different wave absorption methods may be more favorable for one device than another.

		ALC	PLT
$n_e(0)$	$10^{19}/m^3$	100	2
$T_e(0)$	keV	4	4
$T_D(0)$	keV	4	4
Z(eff)		1	3
τ_E	ms	70	20
plasma volume	m^3	.365	4.17
total no. of electrons	10^{19}	18	4.2
P(rf)	MW	4	4
rf power density at r=0	MW/m^3	30	2.6
rf power per ion	keV/sec	137	6000
total internal energy	kJ	189	43
ξ-parameter		3.3	720

The Alcator-C operating territory covers all three wave absorption processes discussed in the previous section -- the majority second harmonic, the minority fundamental cyclotron and the two-ion hybrid resonances heating. The latter two occur at field strengths close to the upper operating limit of the

Alcator-C. A logical progression of the project may be to start with the second harmonic heating of hydrogen plasmas at moderate field strengths and to move on to the second harmonic heating of helium-3 and deuterium plasmas as the machine operating range progresses toward higher field range. The deuteron second harmonic heating will, of course, be influenced by the proton minority and two-ion hybrid resonance heating because of incidentally present proton species.

Our experiments on the Alcator-C have two primary objectives. The first is to deliver at least 4 MW of RF power to the plasma. If a good heating efficiency is attained and if Alcator-C confinement scales as expected, the addition of 4 MW of RF power should take the plasma into the threshold of thermonuclear temperatures. This will enable us to test the continued effectiveness of ICRF heating in these regimes. An antenna design capable of delivering RF power of the order of 1 MW per antenna will have to be developed in order to achieve this goal. The design choice will be limited by constraints imposed by the Alcator-C port structure.

Our second aim is to delineate minimum requirements of the ICRF technique on the tokamak structure. Instead of trying to fit an antenna design to an existing tokamak structure, as has always been the case, we will try to determine to what degree ICRF antennae can be an integral part of tokamak design. Integration of the antennae in the basic tokamak structure will enable designing of higher performance antennae. In order to accomplish

such integration without compromising the tokamak performance, minimum requirements of the ICRF technique on the tokamak structure must be established. We will try to do this in time to make significant contributions to the design of the next generation of tokamaks.

ICRF heating of high density plasmas in the Alcator-C is uniquely suited for achieving these goals. An ICRF antenna in the Alcator-C is expected to have high radiation resistance. This will make circuit loss nearly negligible. Preferential excitation of the higher radial modes makes it possible to bring RF power to the plasma center without a complicated antenna array to define a parallel wavelength. Because energy is rapidly equi-partitioned, the production, and subsequent loss, of highly energetic particles is minimized. In addition, energy deposition in the central part of the plasma may yield an important bonus in that the plasma current profile may be made to peak at the center giving the discharge more favorable MHD characteristics in the so-called saw-tooth regime.

2.3 Expected Heating Results

The expected fractional increase in thermal energy is determined mainly by the RF power coupled into the plasma and by heating efficiency. The achievement of energy increase relatively independent of plasma parameters is another advantage of this heating technique. The plasma thermal energy increase due to RF power applied for a period, t, is given by,

$$W[kJ] = \tau_E[ms] P_6[MW] \eta \, (1 - \exp(-t/\tau_E)) \qquad (2.3.1)$$

where P_6 is the net RF power coupled to the plasma in units of megawatts, $\tau(E)$ the energy confinement time in milliseconds and η is the heating efficiency. Here, the efficiency is defined as the fraction of RF energy converted into plasma thermal energy and retained in the plasma for a period comparable to $\tau(E)$. The energy confinement time of Alcator-C is estimated from the so-called Alcator scaling law(25), $\tau_E[ms]=0.038\bar{n}_{14}\, a[cm]^2$, where $\bar{n}_{14}$ is the line average electron density in units of 10**14/cm**3 and a is the minor radius in cm. In terms of the volume averaged density, $\langle n_{14} \rangle$, and the minor radius in units of 17 cm, a_{17}, the formula takes the following form,

$$\tau_E[ms]=14.6\langle n_{14} \rangle a_{17}^2 \qquad (2.3.2)$$

A high density Alcator-C plasma with $\langle n_{14} \rangle=5$, is expected to have τ_E =73 ms. The total plasma thermal energy (electrons and ions) for parabolic radial density and temperature profiles is given by,

$$W[kJ]= 5.8\langle n_{14} \rangle \left(1 + \frac{T_{eo}}{T_{io}}\right) T_{io}[keV] R_{64}\, a_{17} \qquad (2.3.3)$$

where T_{eo} and T_{io} are the on-axis electron and ion temperatures in keV, and R_{64} the major radius in units of 64 cm. The asymptotic value ($t>3\tau_E$) of the fractional energy increase is therefore given by,

$$\frac{\Delta W}{W} = 2.5 \, \frac{\eta \, P_6[MW]}{T_{io}[keV]\left(1 + \frac{T_{eo}}{T_{io}}\right) R_{64}} \qquad (2.3.4)$$

It is interesting to note that this fraction is ostensibly independent of density. However, it will be shown in the next section that η is influenced significantly by the density.

The minimum expectation of η is 0.3, which was achieved in earlier ATC experiments, but values of 0.6 or higher appear more probable for the Alcator-C plasmas. The table below lists the fractional energy increase for three values of η for each megawatt of RF power coupled and $T_{eo} = T_{io} = 1.0$ keV.

η	1.0	0.8	0.6	0.3
$\Delta W/W$	1.3	1.0	0.75	0.38

Thus, for a total power of 4 MW and $\eta = 0.6$, a four-fold temperature rise, $(1+4\times0.75=4)$, is expected. This temperature rise will bring the plasma to the threshold of thermonuclear regimes. These simple zero-dimensional analyses, however, do not account for the reduction of the ohmic heating power to a nearly negligible value as T_e rises to the 4 keV level. If the initial ohmic heating power of about 1 MW is assumed to be replaced by an additional rf power, the threshold of the thermonuclear regime will be reached when 4 MW is added at $\eta = 0.8$ or 5 MW is added at $\eta = 0.6$. Judging from the PLT experiments these efficiency figures do not appear to be unrealistic values to achieve in the

Alcator-C.

3. PHYSICS OF ICRF HEATING OF HIGH DENSITY PLASMAS

High density plasmas in the Alcator-C provide a particularly attractive environment for ICRF heating because of high radiation resistance and favorable wave field patterns characteristic of such plasmas. To understand these characteristics it is instructive first to look at the flow of energy starting from the RF generator and finally ending up as the plasma thermal energy, identifying at each stage sources of energy loss.

An RF generator operating in a class-C mode is expected to yield about 65 % efficiency, which is higher than that achieved by other techniques of additional heating. Losses in a few-hundred foot long transmission line are small and can be neglected for practical purposes (see Fig. 7). A part of the power is dissipated as heat in the impedance matching network usually required between the transmission line and the antenna, and a part is radiated as waves. As the waves propagate around the torus a part of the wave energy is lost due to the electrical resistance of the walls and the rest is deposited in the plasma in the form of the kinetic energy of ions and electrons. Some of these energetic particles are lost through uncontained orbits before their energy is thermalized and shared with other particles. The thermalized part of the energy appears as increased plasma temperature. Only that part of the energy

deposited in the central core of the plasma is retained for a period comparable to the overall energy confinement time. The part deposited in the peripheries is lost quickly and does not contribute significantly to raising the plasma temperature. We will show in the next few sections that all of these losses are expected to be small in high density Alcator-C plasmas.

3.1 High Radiation Resistance

The impedance-matching network is usually a high-current resonant circuit, and ohmic loss inside it could be significant. The fractional loss in the circuit is determined by the relative sizes of the circuit resistance, R(c), and antenna radiation resistance, R(s). The circuit resistance in many past experiments was typically 0.1-0.2 ohms, while the radiation resistance of small or low-density tokamaks (for example, ST or Macrotor) was typically <0.5 ohms. The fractional power lost was not negligible (0.2/(0.2+0.5)=30 %). The order of magnitude of the circuit loss is the same for larger tokamaks. The radiation resistance is determined, in part, by the antenna design, but increases rapidly with the plasma size and density (e.g., for ATC R(s)=1-2 ohms). The theoretical radiation resistance of the Alcator-C antenna is calculated from a cold, uniform plasma theory at several different densities and is plotted in Fig. 8. The resistance plotted in the figure is the sum of the central six poloidal modes, $-3<m<+2$. It reaches values in excess of 10 ohms for $\langle n_{14} \rangle > 1.0$. "Non-ideal effects", such as

inhomogeneity, thermal effects and finite antenna thickness will probably reduce the actual resistance somewhat, but the circuit loss, caused by circuit resistance of about 0.3 ohms, should not account for more than 5 %.

3.2 Power Branching into Favorable Modes

The RF power radiated as waves is carried by a large number of eigenmodes, each with given radial (l) and poloidal (m) mode numbers. The number of such modes that may propagate in a bounded plasma column is determined by the plasma size and density. In high-density Alcator-C plasmas there are well over 200 such propagating modes. The greatest advantage of high density plasma lies in the existence of a natural selection rule that puts most of the RF power into those modes with the most favorable radial power deposition patterns. The selection occurs naturally in the sense that this can be accomplished without using a complicated phased array of antennae.

The kind of antenna successfully used in many earlier experiments is a metal structure, which is semi-circular or arc-shaped in the poloidal plane, and with a linear dimension comparable to the plasma size. The fact that the relative plasma and antenna sizes are comparable results in the selection of poloidal modes with small eigenmode numbers: a large number of modes can propagate, but those with large poloidal mode numbers carry only a small amount of RF power and are insignificant. The power carried by each mode is proportional to its radiation

resistance. In Fig. 9 the radiation resistance of the Alcator-C antenna -- a single quarter-turn on the larger major radius side of the plasma (see Fig. 15) -- is shown as a function of the poloidal mode number, m. In this case the total radiation resistance is 10.2 ohms, but the central six modes, $-3<m<+2$, account for 96 % of the total resistance.

Each poloidal mode may consist of a number of radial modes. Only the lowest radial mode can propagate in small tokamaks at low densities. In the high-density Alcator-C plasma there are a large number of the higher radial modes for each poloidal mode. The number of possible radial modes is also shown in Fig. 9 as a function of m. An important point to note is that an ICRF antenna couples RF power preferentially to the few highest radial modes of each poloidal mode. This is illustrated in Fig. 10, in which the radiation resistance of radial modes within a given poloidal mode group is plotted as a function of the radial mode number: more than three-quarters of the power radiated through each poloidal mode is carried by the four highest radial modes.

In summary the bulk of the RF power radiated by a simple ICRF antenna is carried by the few highest radial modes of the central poloidal modes with small eigenmode numbers. Because of this "natural selection rule", ICRF heating requires no sophisticated antenna arrays to deliver the power deep into the plasma. This point will be discussed further in the following section in which it will be shown that these modes indeed have

desirable characteristics.

3.3 Radial Wave Field Profiles

The radial power deposition pattern of ICRF heating is determined by the wave field pattern and the wave damping mechanisms. The deuteron second harmonic (DSH) cyclotron damping which puts energy into deuterons is proportional to the square of the perpendicular gradient of an electric field component. The proton fundamental cyclotron (PFC) damping is proportional to the square of the magnitude of an electric field component. In both cases the pertinent field component is the left-hand circularly polarized component. More energy will be transferred from the waves to the plasma at locations where this component and its gradient are large. It is therefore advantageous to have a mode with the radial profile of the left-hand polarized component and its gradient which are peaked in the central core of the plasma. Three cases, with progressively more favorable characteristics, will be discussed in the following three paragraphs.

In Fig. 11 the magnitude of the left-hand(E+) and right-hand(E-) polarized components and the square of the perpendicular derivative of E(+) are shown for the lowest radial mode of m=+1 poloidal mode as a function of the plasma radius. The magnitude of E(+) is small everywhere compared to E(-). The magnitude of E(+) is zero at the plasma center and monotonically increases toward the plasma edge. The gradient is also peaked near the plasma periphery. This is the mode predominant in low

density plasmas in past ICRF experiments (e.g., the ST tokamak). A major portion of the energy deposited near the plasma periphery by this mode will be quickly lost resulting in poor heating efficiencies.

In the higher density plasmas in larger tokamaks, such as the ATC device, the m=0 poloidal mode, with a better radial profile, becomes propagating. However, only the lowest radial mode can be excited under most plasma conditions and the heating efficiency remains relatively low (-30 %). The field patterns of this mode, to be compared to those in Fig. 11, are shown in Fig. 12.

In Fig. 13 the field patterns of the tenth radial mode of the m=0 poloidal mode in the Alcator-C are shown. In contrast to the previous examples, the magnitude of the E(+) component is now a significant fraction of the total field and is concentrated in the plasma interior. This tendency is even stronger for the perpendicular gradient. The concentration of energy deposition in the plasma center is further accentuated by the fact that both the plasma density and the temperature are peaked there. The minority damping is proportional to the density and the second harmonic damping, to the product of the density and ion temperature.

These theoretical observations are the basis for anticipating substantially higher heating efficiencies in the high density Alcator-C plasma than those obtained in previous

experiments.

3.4 Toroidal Resonance

Waves generated by an antenna in a toroidal plasma propagate around the torus and return to the antenna location. If the wave damping is strong, the amplitude of the waves after they circumnavigate the torus is small and their effects on the antenna are insignificant. The antenna sees essentially an infinitely long plasma, and the antenna loading resistance is practically identical to the radiation resistance. If the damping is weak, on the other hand, the interference of the circumnavigating wave fields is strong and the antenna loading resistance for an individual mode varies widely as the toroidal cavity undergoes successive resonances and anti-resonances with changing plasma density. Such toroidal eigenmode resonances were observed in many experiments and their general features were found in agreement with theories of fast wave propagation.

If there are only a few propagating modes, as is the case in low density plasmas, it would be necessary to track a toroidal resonance peak to avoid a wide swing of the transmitter load impedance as well as to take advantage of high peak loading resistance to ensure high power coupling without voltage breakdown problems. In high density plasmas the loading resistance of an individual mode may vary widely, but overlapping of many modes produces high loading resistance which is nearly steady in time. This tendency toward smoother loading resistance

variation was observed at high densities in the ATC device. Under these circumstances the mode tracking is both unnecessary and impracticable. This is another advantage which high density Alcator-C experiments can exploit.

3.5 Wave Damping Mechanisms

Knowledge of the wave damping mechanism is very important, if the experimental observations in the existing tokamaks are to be reliably extrapolated to future experiments and reactors. The physics of wave damping can be complicated when there are more than one species of ions in the plasma. For example, a small quantity of protons inadvertently present in a deuterium plasma causes several wave absorption mechanisms to be present at the same time. It is also possible, however, to take advantage of such effects and add minority species to control the division of rf power deposited among various species. There are three wave absorption mechanisms identified for the fast waves in the ion cyclotron range of frequencies: (1)majority ion species second harmonic(SH) cyclotron damping, (2)minority ion species fundamental cyclotron(FC) damping, and (3)mode conversion(MC) damping at the two-ion hybrid resonance.

The second harmonic damping occurs in its pure form only in plasmas uncontaminated by impurities having their cyclotron frequencies close to the second harmonic cyclotron frequency of the majority species. The SH heating of hydrogen and helium-3 plasmas are such examples. In deuterium plasmas, in which a

small amount of hydrogen is invariably found, the deuteron SH resonance, proton FC resonance and deuteron-proton hybrid resonance occur in close physical proximity. As a result, the pure SH damping is overshadowed by the FC damping and the two-ion hybrid resoance that enhances both the SH and FC damping. The pure SH damping will be the primary interest of the Alcator-C project, although both the minority FC and MC damping conditions may be obtained at high toroidal field strengths.

According to a warm-plasma, slab-geometry analysis the power absorbed per unit height and depth of the slab by the deuteron SH damping is given by(26),

$$P_{II} = 4\pi R_c \left(\frac{\omega_{PD}^2}{\omega}\right)\frac{\epsilon_0}{4}|E_+(x)|^2_{x=x_c}\left(\frac{\rho_D}{2a}\right)^2 J_{II} \qquad (3.5.1)$$

where

$$J_{II} = \frac{2}{\pi^{1/2}}\int_0^\infty d\zeta_D |\mathcal{F}(\zeta_D)|^2 \exp - \zeta_D^2 \qquad (3.5.2)$$

$$\mathcal{F}(x) = a[dE_+(x)/dx]/E_+(x_c) \qquad (3.5.3)$$

$$\zeta_M = \left(\frac{u_\parallel}{v_M}\right)\frac{(x - x_c)}{R_c} \qquad (3.5.4)$$

The function, $\mathcal{F}(x)$, in the integrand is the dimensionless gradient of the left-hand polarized component E(+) of the wave field normalized by the value of E(+) at the cyclotron resonance surface. For the pure SH damping $J_{II} = (k_A a)^2$ is a good

approximation, where k_A is the Alfvén wave number. The absorbed power is proportional to the deuteron density, the temperature and the square of the gradient of the E(+)-field approximated by $k_A^2 |E(+)|^2$ and evaluated on the cyclotron surface. The product of these three quantities is, by as much as two orders of magnitude, greater in the Alcator-C than in any other tokamaks in which ICRF heating was attempted. It is for this reason that the pure SH damping in hydrogen or helium-3 plasmas can be a viable absorption mechanism for plasma heating in the Alcator-C.

The table below lists the wave damping lengths of several modes normalized by the toroidal circumference for the Alcator-C deuterium plasma at $\langle n_{14} \rangle = 2.5$. l, m and n are the radial, poloidal and toroidal mode numbers, respectively. The tabulated numbers for L(d)/L and L(W)/L signify the number of times the waves go around the torus before their amplitudes e-fold due to the pure SH cyclotron damping and wall resistive damping, respectively. The wall damping length is calculated on the assumption that the actual wall loss is greater than the loss in ideally smooth stainless-steel walls by a factor of twenty(26). Energy loss due to the wall resistance is significant for low radial modes compared to the energy absorption by the plasma. The wall loss is much smaller, however, for high radial modes which carry most of the RF power. We anticipate from these calculations that in high density Alcator-C plasmas the pure SH cyclotron damping -- normally a weak damping mechanism at low densities -- will be far stronger than the wall resistive

damping, and that most of the energy will be absorbed by the plasma.

l	m	n	L(D)/L	L(W)/L
1	0	35	36	328
3	0	28	4.1	52
5	0	11	0.7	17
1	1	36	95	709
3	1	30	6.2	62
5	1	17	1.2	23

The minority FC damping occurs when a small concentration of a resonant ion species is present in a majority non-resonant ion species. The minority FC heating was studied intensively in the recent PLT experiments(15). The power absorbed per unit height and depth of the slab by the proton FC damping is given by(26),

$$P_I = 4\pi R_c \left(\frac{\omega_{PH}^2}{\omega}\right)\frac{\epsilon_0}{4}|E_+(x)|^2_{x=x_c} J_I \qquad (3.5.5)$$

where

$$J_I = \frac{2}{\pi^{1/2}} \int_0^\infty d\zeta_H |\mathcal{E}(\zeta_H)|^2 \exp - \zeta_H^2 \qquad (3.5.6)$$

$$\mathcal{E}(x) = E_+(x)/E_+(x_c) \qquad (3.5.7)$$

The function, $\mathcal{E}(x)$, in the integrand is E(+) normalized with respect to its value at the cyclotron resonance surface. The power absorbed by the FC damping is proportional to the product of the proton density and the square of the magnitude of the E(+) field.

The minority FC damping is influenced by the inevitable presence of the two-ion hybrid resonance in the vicinity of the cyclotron resonance. This comes about because the linear polarization of the electrostatic hybrid resonance alters the wave field polarization in the vicinity of the cyclotron layer in favor of the left-hand circularly polarized component(13). The value of the integral given in Eq. (3.5.6) is the enhancement factor. In the special case of deuterium plasma contaminated by hydrogen, the deuteron SH damping is also enhanced by the hybrid resonance because the deuteron SH and proton FC frequencies are identical. The enhancement factor is given by $J_{II}/(k_A\, a)^2$ for this case. Both of these enhancement factors, however, tend asymptotically to unity at higher densities. The enhancement factors are listed below for deuteron SH and proton FC damping in deuterium plasmas as a function of the density(26).

$\langle n(14)\rangle$	0.08	0.15	0.25	0.35
DSH	590	54	5.2	1.1
PFC	15	3.1	1.8	1.3

These values were obtained for plasma conditions prevailing in the ATC tokamak. Both enhancement factors approach unity for densities above $0.35 \times 10^{14}/cm^3$ and effects of the hybrid resonance in enhancing the cyclotron damping become insignificant.

Under the conditions in which the enhancement of the cyclotron damping is insignificant, the ratio of the power absorbed by the majority SH damping to that by the minority FC damping can be calculated from Eq. (3.5.1) and (3.5.5),

$$(P_{II}/P_I) = (A_{II}/A_I)(n_{II}/n_I)(v_D/V_A) \qquad (7)$$

where the subscripts, I and II, refer to quantities pertinent to the minority and majority species, respectively. The square of the ratio, v_D/V_A, of the majority ion thermal speed to the Alfvén speed can also be written as the ratio, β_D, of the majority ion thermal to magnetic pressure. Thus, the deuterons will absorb more energy than the protons, only when the proton concentration is less than one half of β_D. ($\beta_D[\%] = 4.0 n_D[10^{21}/m^3] T_D[keV]$ may reach a few percent at the plasma center.) The power absorbed directly by the deuterons can become significant compared with that absorbed by the protons in the minority heating of high density Alcator-C plasmas.

In Section 3.3 the radial profile of the magnitude and perpendicular gradient of E(+) field are shown to be peaked near the plasma center for high radial modes that carry most of the rf power. It should be clear from the discussion above that the

power deposition profiles of the majority SH and minority FC heating are very favorable for efficient heating. This is especially true for the SH heating because the peaked field gradient profile is further accentuated by the peaked radial profile of nT.

The MC damping at the two-ion hybrid resonance occurs in plasmas made up of two ion species of comparable concentrations(10). The fast waves are damped because a part of their energy is converted to the energy of shorter wavelength electrostatic waves. The MC damping was the focal point of the recent investigations by TFR group. Gross qualitative behavior of heating was found consistent with theoretical expectations. Details of the damping of the short wavelength mode are, however, not well known at this time.

The physical environment in which wave absorption takes place in the hybrid layer is similar to the classical "Budden tunneling" problem -- back-to-back presence of linear and singular turning points(see Ref. (27)). The tunneling factor that characterizes the transmission, reflection and absorption as the waves pass through the layer once, was first obtained by Swanson(10). Many different expressions have since been obtained by many researchers(11)(12) corresponding to varying degrees of sophistication of the physical model. The fate of the energy transferred to the short wavelength mode -- whether it is deposited into the electrons through Landau damping, or into the

ions through cyclotron damping -- depends delicately on the rotational transform of the toroidal magnetic field(11). The total amount of the power removed from the fast waves can be calculated, however, based upon the simplest Budden's treatment of a second order differential equation. The absorbed power is determined mainly by the plasma density and is essentially independent of thermal effects. Such calculations using reactor plasma parameters show that the waves incident on the hybrid layer from the low field side should be nearly totally reflected and the waves incident from the high field side nearly totally absorbed(10). This would imply that an antenna placed on the low field side is not suitable for reactor plasma heating using mode conversion damping. The Alcator-C is the only currently available tokamak in which such predictions can be tested.

3.6 Losses Due to Uncontained Orbits

When the fast waves are damped, their energy is converted to the thermal energy of plasma particles. Under the minority species heating a large amount of power is shared among a small number of ions, and a large suprathermal tail is often formed in the ion energy distribution. These energetic ions are more likely to be lost through uncontained orbits. The rate of production of such energetic ions is, however, related to the magnitude of the drag experienced by the ions, and thus becomes small at high densities.

In Fig. 4 the proton distribution observed in the PLT minority heating experiments is compared with the theoretical prediction (shown by the solid curve) based upon Stix's theory(16). Reasonable agreement between the experiments and theory suggests the use of the theory for predicting production of the tail particles in future experiments.

Results of calculations for Alcator-C and PLT plasmas are summarized in Fig. 14. The lower curve for the Alcator-C, marked ξ=1.6, is the proton distribution when 4 MW of rf power are applied at T=T(i)=T(e)=1 keV. The upper curve, marked ξ=3.3, is for the same rf power but at T=4 keV. The upper dotted curve, marked ξ=719, for the PLT is the proton distribution when 4 MW of rf power are applied at T=4 keV, and the lower curve, marked ξ=36, is when rf power is 400 kW and T=1 keV. The latter case is similar to the conditions encountered in the recent PLT experiments. The on-axis density is assumed to be $10^{21}/m^3$ for the Alcator-C and $2\times10^{19}/m^3$ for the PLT.

The PLT, ξ=719 case shows that a large number of protons is at very high energy, and that the minority heating is likely to be poor under these conditions. The PLT, ξ=36 case is much improved over the previous case. In fact, satisfactory heating was observed in the actual experiments, although there were some evidence that some of these particles were uncontained and were contributing to the power loss(15). The Alcator-C, ξ=3.3 case is much improved compared to the PLT, ξ=36 case. Thus, we may surmise that production of energetic protons in the minority

heating is much less in the Alcator-C at P(rf)=4 MW than in the PLT at P(rf)=400 kW.

There are two kinds of energetic particle loss that need be considered. One is the loss due to toroidally trapped particles with too large banana orbits, and the other is due to localized particles trapped in field ripples. The loss-cone energies for the banana orbits are proportional to the square of the plasma current. At a plasma current of one megaampere the minimum loss-cone enegy in the plasma center is well above 1 MeV, and the loss due to this source in the Alcator-C should be negligible. The toroidal field ripple in the Alcator-C is also believed to be small (about 1 %). Because of a slight variation of the magnitude of the field over the ripple width caused by the rotational transform, the ripples may in fact be incapable of trapping any particles(28).

3.7 Antenna Design

One area in which high density plasmas indirectly exact a price for the advantages cited throughout the previous sections is the compactness of the Alcator-C device with its limited access ports. It is a technical challenge to devise means of delivering through these ports RF power high enough to heat a large number of plasma particles. The first goal of the antenna research program, primarily in FY80, will be concerned with devising a design that is compatible with the constraints imposed by the Alcator-C port structure and that is capable of radiating

an RF power of the order of 1 MW per antenna.

Antennas that are usable in the severe thermonuclear environment of a reactor are expected to have a rugged and simple structure. The antenna research program will shift emphasis during its second phase, mainly in FY's 81 and 82, with a new goal of finding the simplest possible structure that functions satisfactorily as an antenna. In the development process, it should become clear what kind of tokamak structural changes will permit installation of higher performance antennae, and to what extent the antenna can be an integral part of the tokamak structure. These possible modifications, that can be incorporated in future tokamak design, will, however, have to be made without compromising the basic tokamak performance. Need for compatibility between high performing ICRF antennae and tokamaks with good operating characteristics demands determination of the minimum requirements of ICRF technique on the tokamak design. The requirements are not necessarily limited to the access port size or shape. They may have impact on the mechanical and electrical characteristics of limiters, vacuum vessel and magnets.

In Fig. 15 the design of the first antenna developed for the Alcator-C is shown. It consists essentially of an arc-shaped metal member subtending a poloidal angle of 90 degrees and a pair of protective limiters placed on either side of the antenna. The design evolved out ot the earlier ATC antenna, but unlike the ATC antenna it has no ceramic elements around the antenna proper or

on the faces of the limiters. In this sense the current design represents a step forward toward the ultimate design. The antenna is movable in the major radial direction.

The whole structure inside the vacuum vessel will be made largely of stainless-steel and molybdenum. The ATC antenna was made of copper. The antenna proper and the return current strap are made of stainless-steel sublimated with a thin layer of molybdenum for good RF electrical conductivity. A thermocouple, a current probe and an electrostatic probe will be installed to diagnose the antenna performance. These elements are not shown in Fig. 15.

The coaxial transmission line segments, to which the antenna proper are connected, are 1 5/8 inch in diameter and their characteristic impedance is 75 Ohm. The ceramic vacuum feed-throughs are placed near the location where the lines penetrate through the Alcator vacuum flange. Outside the vacuum vessel the transmission lines are enlarged to 3 1/8 inches in diameter, and the both lines are terminated in short circuits. The length of the lines is varied by means of adjustable-length sections in order to bring the entire, ten half-wavelength long line segment into a resonance. One of the voltage minimums of the resulting standing wave is located at the antenna center. The vacuum feed-throughs are located at voltage minimums adjacent to the one at the antenna center, and all adjustable-length sections are located near current minimums. The two halves of this resonant line are driven in a push-pull manner through a

180-degree hybrid coupler.

3.8 Summary of Advantages of Alcator-C Experiments

The advantages of the proposed Alcator-C experiments can be summarized as follows:

(1)The Alcator-C is likely to be the first tokamak that can take full advantage of the second harmonic cyclotron heating -- probably the most suited of the three wave absorption mechanisms in reactor applications.

(2)The Alcator-C can be heated efficiently by the minority species heating -- the most thoroughly tested of the three wave absorption mechanisms.

(3)The Alcator-C is the only existing tokamak that can provide convincing proof for the theoretical predictions on the two-ion hybrid heating.

All of these advantages stem from the high densities that the Alcator-C can attain.

4. ENGINEERING

The bulk of the equipment needed for the project was obtained as surplus from the United States Air Force. The original equipment was a radar transmitter system deployed on the island of Shemya. The major part of the system was acquired by the Department of Energy and then was assigned to M.I.T. for use in the ICRF project. The transferred items included amplifier chains, coaxial transmission lines and miscellaneous RF and electrical components. The power supplies, configured for high-power, short-pulse operations, were judged unsuitable for our purposes and were not acquired. Some selected RF components from other USAF radar stations have since been added to the original Shemya equipment.

The engineering aspect of the project consists of the following three principal tasks:

(1) installation, refurbishing, minor modifications and tuning of rf amplifiers; miscellaneous engineering tasks;

(2) procurement and installation of a DC power supply for high power amplifiers (HPA) and intermediate power amplifiers (IPA);

(3) mechanical and electrical modifications of amplifier chains for lower frequency operations.

4.1 Amplifiers

There are twelve amplifier chains which will be available for this project. Each chain consists of HPA, IPA and low level driver (LLD) stages. One complete chain is on loan to the University of California at Los Angeles (UCLA) and one IPA is on loan to Princeton Plasma Physics Laboratory (PPPL). At present there are ten complete amplifier chains with four HPA and five IPA vacuum tubes at hand. The amplifiers can be tuned for frequencies between 180 and 216 MHz. These frequencies correspond to the deuteron second harmonic (DSH) cyclotron resonance at on-axis toroidal field strengths of 118 and 142 kG, respectively, or, to the proton second harmonic (PSH) cyclotron resonance at 59.0 and 72.2 kG, respectively.

Four amplifier chains are now installed in place and refurbishing, minor modification and tuning work is in progress. Each amplifier chain, in its original configuration, is capable of generating 2.5 MW of RF power for a short period (3 ms). For long pulse operations (a few hundred milliseconds) the capability of the amplifier chain is not yet well defined. Judging from an earlier CW test by the manufacturer of the HPA tube, however, an RF output power of 1 MW is considered feasible if a DC power supply for long pulse operation is available. Thus, the capability of all four amplifier chains is nominally 4 MW.

The experience from the ATC experiments indicates that the best heating results when the cyclotron resonant surface is placed on the larger major radius side of the magnetic axis by a small distance. This requirement and the operating frequency range of the amplifiers mean that hydrogen heating experiments should be conducted at moderate field strengths (65-79 kG) and deuterium experiments at very high field strengths (130-158 kG). Routine operations in the higher field range involve considerable risk of a component failure and premature termination of the device life. The repetition rate of plasma discharge will also be slow under such operating conditions. For these reasons modification of the amplifiers for lower frequency is planned. The modification involves lengthening of the input and output cavities of the IPA and HPA amplifiers. A fifteen percent reduction in the lower frequency limit to 150 MHz would permit deuteron second harmonic, proton minority and deuteron-proton hybrid heating experiments at 100 kG range.

It is planned that at least one amplifier chain will be tuned and operational at a 1 MW level by January, 1980. The HPA of this amplifier chain will be supplied with DC power from a lower hybrid heating power supply (See below). The other three chains will be made ready during 1980. A decision on the amplifier modification must be reached by the summer, 1980, in order to complete the redesign and fabrication of the modified circuits in a timely manner. In FY81 and FY82 more amplifiers will be brought into operation, if experimentation at higher

power levels is warranted.

There are only four HPA vacuum tubes at hand. Three of them are serviceable and one is damaged but probably repairable. For the IPA stage five vacuum tubes are available. Unless more tubes become available as surplus, at leat one HPA tube must be purchased before all four amplifier chains can be made operational. In order to provide for a spare in case of tube failure and to bring more amplifiers into operation in the future, funds are allotted for purchasing several more HPA and IPA tubes in the coming three years.

4.2 DC Power Supplies

There is more than one option in securing DC power for HPA's and IPA's. In this section the preferred option is described. This plan calls for procurement of a new 10 MW DC power supply for the long range use and adaptation of a Lower Hybrid Heating (LHH) power supply unit as an interim solution. The budget presented in the next section is based on this plan. Another option, one that will provide a total RF power of about 1.6 MW initially and 6.4 MW in the future, will be discussed in the next section. In this plan the entire LHH power supply will be shared by the ICRF project.

(a)Lower Hybrid Heating Power Supply

One unit of the lower hybrid heating power supply, the so-called Lincoln Laboratory (LL) supply, will be utilized on

an interim basis, between January, 1980 and the arrival of the new power supply in the fall, 1980. The LL supply is capable of powering one HPA at about an 0.8 MW level. The necessary buss work, filter/crowbar assembly and associated controls will be provided by January, 1980. The LL supply has poor voltage regulation ("soft supply") and the output voltage droops by about 20 % (RF power by 40 %) as the current is drawn. In order to avoid an excessive voltage droop, a shunt voltage regulator will be installed to pre-load the power supply. Provision to procure one unit of the regulator is made in FY80. An existing capacitor bank will be used to power one unit of IPA for moderately long pulse operation.

(b)10 MW Power Supply

The proposed new power supply consists of two identical units, each capable of delivering 5 MWDC. The supply will be designed for powering both HPA's and IPA's. Each power supply unit consists of a fast-acting protective AC switch gear, transformer/rectifier assembly and filter/crowbar assembly. Some important parameters of the power supply are listed below.

Switch Gear

Voltage	13.8 kVAC
Current	1200 ampere Continuous
Interrupting time	1.5 Cycles at 60 Hz

Transformer/Rectifier Assembly

No. of Primary Inputs	1
No. of Secondary Outputs	2
Voltage Regulation	5 %
Primary Voltage	13.8 kVAC
Secondary Voltage and Current	
No. 1	24 kVDC at 200 amperes (no-load taps at 22, 26 and 28 kV)
No. 2	10 kVDC at 20 amperes (no-load taps at 9, 11 and 12 kV)

Filter/Crowbar Assembly

No. of Inputs	1
No. of Outputs	3
Filter Capacitance	45 microfarads
Capacitor Voltage Rating	33 kVDC
Ignitron Stand-Off Voltage	50 kVDC
Charge Handling Capacity	100 coulombs
Max. Fault Energy	6 joules

All of these components, except the filter/crowbar assemblies, will be placed outdoors on a strip of land behind the Magnet Laboratory reserved for this purpose. The output voltages of both HPA and IPA secondaries can be adjusted by means of no-load taps for optimum amplifier operation. The filter/crowbar assembly, used in conjunction with the LL supply, will be utilized in one leg of the new supply.

Another identical filter/crowbar assembly will be built for the other leg.

According to the quotations by equipment manufacturers the delivery time and cost of two transformer/rectifier units are 26 weeks and $183,200, those for two switches 40 weeks and $53,750, and those for two crobar/filter assemblies 12 weeks and $48,500, respectively. In order to have the power supply ready in the fall of 1980, the procurement procedures must be initiated immediately. Preparation of the power supply site can be accomplished within the waiting time for the other components.

This option of a dedicated power supply has an obvious advantage of a tailor-made system with various built-in flexibilities to optimize the amplifier operation. It also eliminates the need for building a separate IPA power supply and avoids possibly difficult scheduling problems when modifications of the LH supply units are made. The additional cost of securing a separate supply may not be large because considerable modifications of the LHH supply may be needed to utilize it.

4.3 Lower Hybrid Power Supply Utilization

Some pertinent points will be discussed in this section on sharing the power supply built for the LHH project. The LHH power supply consists of four units, the Lincoln Laboraroty (LL) unit and three new units built by the Universal Voltronics

Corporation (UVC). Utilization of the LL unit and the UVC unit will be discussed separately.

The LL unit consists of two sub-units. For the LHH project these sub-units are connected in series and produce an output voltage of 65 kV. The voltage can be lowered to 24 kV suitable for the ICRF use by means of an Inductrol connected to the primary side of the unit. The maximum current is, however, limited to 60 A by the rectifier component of the unit. The maximum output power available for the ICRF purposes is limited to 1.5 MWDC (approx. 800kWRF). The utilization of the LHH unit discussed in the previous section refers to this series configuration.

It is possible, however, to configure the LHH sub-units in parallel connection, which results in two outputs of 1.5 MWDC each. The two outputs can not, however, be tied together and all components downstream of the units, including filter/crowbar, voltage regulator, buss work and HPA must be duplicated. Approximately two man-months of engineering time and four man-months of electrician time will be needed for rearranging the output cable connections, installing an additional cable through an underground conduit and modifying the control circuits.

The parallel connection of the LL sub-units will provide a DC power of 3 MW. This will be sufficient to power two separate HPA's at an RF power of approximately 800 kW each. In order to utilize the LL supply as a long term solution to ICRF power

supply needs, a separate power supply to feed at least two IPA for long pulse operation will also have to be procured.

Each UVC unit is similarly made up of two sub-units connected in series for the LHH purposes. The UVC supply is a "stiff" supply and the output voltage is regulated to 4.5 %, which is also adequate for the ICRF purposes. Unlike the LL unit, however, there are no means of adjusting the output voltage continuously. Only way to lower the voltage is to connect the sub-units in parallel. When the sub-units are connected in parallel, two independent outputs with a fixed voltage in the neighborhood of 35 kV will result. The two outputs can not be combined, and all components downstream of the supply sub-units must be duplicated, as in the LL unit case. This output voltage is too high for the HPA, and series voltage regulators must be used to reduce it by about 10 kV. This would result in loss of about one-third of the DC power in the series tubes.

In the event all four LHH power supply units are configured in parallel connection for the ICRF purposes, the final system may consist of eight independent channels, each having its own filter/crowbar assembly, voltage regulator and buss work. The system will power eight HPA's, each generating about 800 kW of RF power. An independent power supply is needed to power eight IPA's, with a total DC power of about 1.5 MW. Information on the cost of building these components, except the filter/crowbar assemblies, is not available at this moment. The lowest quoted price for filter/crowbar assembly is $33 thousand for one unit

and $48.5 thousand for two units. The price of each of the voltage regulators are estimated to range from $50 to $130 thousand.

If the ICRF project is ultimately to reach the 4-5 MWRF level of operation, the cost of a system that would result from the adaptation of the LHH power supply may be substantial.

4.4 Miscellaneous Engineering Tasks

Other miscellaneous enginnering tasks include fabrication of a heat exchanger, rearrangement of transmission lines, modification of power combiners, installation of dummy loads and building of a data acquisition system.

REFERENCES

(1)Rothman, M.A., Sinclair, R.M., Brown, I.G. and Hosea, J.C., "Ion Cyclotron Heating in the Model C Stellarator", Phys. Fluid 12(1969)2211

(2)Vdovin, V.L., Zinov'ev, O.A., Ivanov, A.A., Kozorovitskii, L.L., Parail, V.V., Rakhimbabaev, Ya.R. and Rusanov, V.D., "Excitation of Magnetosonic Resonance in the Tokamak Plasma", ZhETF Pis. Red. 14(1971)228
Ivanov, N.V., Kovan, I.A. and Los', E.V., "Excitation of the Spectrum of Natural Oscillations of the Plasma Pinch in the Tokamak TO-1", Translation from At. Energ. 32(1972)453

(3)Adam, J. and Samain, A., Report EUR-CEA-FC-579(1971), Association Euratom-CEA, Fontenay-Aux-Roses

(4)Vdovin, V.L., Zinov'ev, O.A., Ivanov, A.A., Kozorovitskii, L.L., Krotov, M.F., Parail, V.V., Rakhimbabaev, Ya.R., Rusanov, V.D. and Shapotkovskii, N.V., Sov. Phys. JETP Lett. 17(1973)2

(5)Adam, J., Chance, M., Eubank, H., Getty, W., Hinnov, E., Hooke, W., Hosea, J., Jobes, F., Perkins, F., Sinclair, R., Sperling, J. and Takahashi, H., "Wave Generation and Heating in the ST Tokamak at the Fundamental and Harmonic Ion Cyclotron Frequencies", in Proc. of the 5th Conf. on Plasma Physics and Cont. Nuclear Fusion Res., Tokyo, 1974, (INt. Atomic Energy Agency, Vienna), 1975, Vol. II, p.65

(6)Ivanov, N.V., Kovan, I.A., in Proc. of the 5th Conf. on Plasma Physics and Cont. Nuclear Fusion Res., Tokyo, 1974, (Int. Atomic Energy Agency, Vienna), 1975, Paper IAEA-CN-33/A9-5

(7)Takahashi, H., Daughney, C.C., Ellis, R.A.Jr., Goldston, R.J., Hsuan, H., Nagashima, T., Paoloni, F.J., Sivo, A.J. and Suckewer, S., "Ion Heating in ATC Tokamak in the Ion Cyclotron Range of Frequencies", Phys. Rev. Lett. 39(1977)31

(8)TFR Group, "Excitation and Damping of the Fast Magnetosonic Wave in TFR near the Harmonic Cyclotron Frequency", 3rd Int. Meeting on Theo. and Exp. Aspects of Heating Toroidal Plasmas, Vol.I, p.87 (Commissariat A L'Energie Atomique, Grenoble), 1976

(9)Greenough, N., Palolni, F.J. and Takahashi, H., "Generation, Propagation and Damping of Fast Waves in Deuterium Plasmas in the ATC Tokamak", Bull. Am. Phys. Soc. 21(1976)1157, Paper 8C-9
Takahashi, H., See Ref.(13) below.

(10)Swanson, D.G., "Mode Conversion and Tunneling at the Two-Ion

Hybrid Resonance", Phys. Rev. Lett. 36(1976)316

(11)Perkins, F.W., "Heating Tokamaks via the Ion-Cyclotron and Ion-Ion Hybrid Resonances", Nucl. Fusion 17(1977)1197

(12)Jacquinot, J., McVey, B.D. and Scharer, J.E., "Mode Conversion of the Fast Magnetosonic Wave in a Deuterium-Hydrogen Tokamak Plasma", Phys. Rev. Lett. 39(1977)88
Takahashi, H., See Ref.(13) below.
Vdovin, V.L., Shapotkovsky, N.V. and Chesnokov, A.V. "Ion-Ion Hybrid Resonance and Alfven Waves in Tokamak TM-1-HF", Int. Conference on Ionization Phenomena and Gas Discharges, Prague, 1977

(13)Takahashi, H., "ICRF Heating in Tokamaks", J. de Physique, Coll. C6, suppl. au n 12, Tome 38(1977)171

(14)Colestock, P., private communications

(15)Hosea, J., Arunasalam, V., Bernabei, S., Bitter, M., Boyd, D., Bretz, N., Chrien, R., Cohen, S., Colestock, P., Davis, S., Dimock, D., Dylla, F., Eames, D., Efthimion, P., Eubank, H., Goldston, R., Grisham, L., Hinnov, E., Hsuan, H., Hwang, D., Jobes, F., Johnson, D., Kaita, R., Lawson, J., Mazzucato, E., McNeil, D., Medley, S., Meservey, E., Mueller, D., Sauthoff, F., Schilling, G., Schivell, J., Schmidt, G., Sivo, A., Stauffer, F., Stodiek, W., Stooksberry, R., Strachan, J., Suckewer, S., Tait, G., Thompson, H. and von Goeler, S., "Fast Wave Heating in the Princeton Large Torus", Reprort PPPL-1588, Princeton Plasma Physics Laboratory, 1979

(16)Stix, T.H., "Fast-Wave Heating of a Two-Component Plasma", Nucl. Fusion(1975)737

(17)TFR Group, "ICRF Heating in TFR at the Ion-Ion Hybrid Resonance", European Conference Paper

(18)Kovan, I.A., Paper Presented at U.S.-U.S.S.R. Workshop on High Frequency Heating, Sukhumi, 1978;
See also: Ivanov, N.V., Kovan, I.A., Sokolov, Y.V. and Chudnovskii, A.N., "Ion Cyclotron Heating of T-4 Tokamak", Fizika Plasmy 4(1978)1211

(ref19)DIVA Group, "Preliminary Results of ICRF Heating in DIVA", Unpublished Note, 1979, Japan Atomic Energy Research Institute; See also
Kimura, H., Odajima, K., Sengoku, S., Iizuka, S., Sugie, T., Takahashi, K., Yamauchi, T., Kumagai, K., Takeuchi, H., Matsumoto, H., Matsuda, T., Ohasa, K., Nagami, M., Yamamoto, S., Nagashima, T., Maeda, H. and Shimomura, Y., "ICRF Heating in DIVA", Report JAERI-M8429, Sept., 1979, Japan Atomic Energy Research Institute

(20)Taylor, R.J. and Morales, G.J., "ICRF Heating in Macrotor", Bull. Am. Phys. Soc. 24(1979)992, Paper 4F7

(21)Green, G.J. and Gould, R.W., "Coupling Efficiency to ICRF Toroidal Eigenmodes and Transmission Between Two Identical Antennas", Bull. Am. Phys. Soc. 24(1979)1062, Paper 7R8

(22)Coleman, P.D., Blackwell, B.D., Beckrich, S.R., Kristiansen, M. and Hagler, M.O., "Measurements of Toroidal Eigenmode Field Structures in the Texas Tech Tokamak", Bull. Am. Phys. Soc. 24(1979)1062, Paper 7R9

(23)Gaudreau, M.P.J., Sansone, M., Shulsinger, D.H., Besen, M., Abbanat, B. and Parker, R.R., "Preliminary ICRH Results on the Alcator-A Tokamak", Bull. Am. Phys. Soc. 24(1979)1062, Paper 7R7

(24)Messiaen, A.M., Weynants, R.R., Bhatnagar, V.P. and Vandenplas, P.E., "Ion-Ion Hybrid Damping of Magneto-Acoustic Resonances", Physics Letters 71A(1979)431

(25)Gondhaleker, A.,
(26)Takahashi, H., "ICRF Heating and Wave Generation in the ATC Tokamak", Princeton Plasma Physics Lab., PPPL-1545, April, 1979

(27)Stix, T.H., Theory of Plasma Waves, McGraw-Hill, New York, 1962

(28)Schuss, J., private communication, M.I.T., 1979

FIGURE CAPTIONS

Fig. 1 Variation in antenna loading resistance as a function of magnetic field strength (expressed in terms of the ion cyclotron to wave frequency ratio) and time (or equivalently plasma density).
The top diagram is a tone plot obtained experimentally. Darker tone indicates high loading resistance caused by the occurrence of toroidal eigenmode resonances. The bottom diagram shows the theoretical prediction of the occurrence of eigenmode resonances(5).

Fig. 2 Experimentally measured radial variation of the ion temperature with and without an ICRF heating pulse. Measurements made by four independent diagnostics are shown to be consistent among themselves(15).

Fig. 3 Measured temperature rise as a function of rf power for two different cases, one with proton minority and the other with helium-3 minority, both in deuteron majority plasmas(15).

Fig. 4 Comparison of observed and predicted proton tail distribution in PLT minority species heating(15).

Fig. 5 Two-ion hybrid resonance heating in TFR(17). The top diagram shows variations in neutron counting rate as the two-ion hybrid and proton cyclotron resonance layers are moved across the plasma cross-section. The bottom diagram shows the observed temperature rise normalized by the rf power as a function of the hybrid resonance layer location.

Fig. 6 Operating regimes of ICRF experiments.
Regions of frequency-magnetic field plane are indicated for three major ICRF heating experiments. PLT-1 and PLT-2 refer to experiments with two different generators.

Fig. 7 Energy Flow and Loss
Sources of energy loss are depicted along the route of energy flow from generator to plasma. The resistive loss in the matching network is the first source of loss encountered. The remaining energy will be radiated as waves in different modes. Part of the energy is lost due to wall resistance. Energetic particles in uncontained orbits produced by the waves are another source of energy loss. Energy deposited in the periphery of the plasma is quickly conducted away. All of these losses are expected to be small in high density plasmas in the Alcator-C.

Fig. 8 The radiation resistance, R(s), is plotted for several different values of plasma density. The resistance is the sum of contributions from the central six poloidal modes

with $-3<m<+2$.

Fig. 9 The radiation resistance, R(s), is plotted as a function of the poloidal mode number, m. Each poloidal mode may consist of a large number of radial modes. The total number of radial modes possible is also plotted as a function of m. However, the loading resistance for a 90-degree antenna falls off rapidly with increasing m and for the purpose of calculating R(s), only $-3<m<+2$ need be considered. The resistances of all radial modes with the same poloidal number are summed to show the total resistance of the poloidal mode.

Fig. 10 The radiation resistances, R(s), of an Alcator-C antenna, due to excitation of individual radial modes, are plotted as a function of the radial mode number, l. All radial modes with a given poloidal mode number, m, are grouped together and are shown by a single curve. More than three-quarters of the power radiated through each poloidal mode are carried by the four highest radial modes.

Fig. 11 The field patterns are shown for the first radial mode of the m=+1 poloidal mode when the m=+1 Fourier component of the antenna current equals one ampere. The abscissa is the plasma radius normalized by the vessel radius and is common to both top and bottom graphs. (a)The amplitude of the left (E(+)) and right (E(-)) hand circularly polarized electric field components. E(+) is small everywhere. It is zero at the center and increases monotonically toward the plasma edge, indicating an unfavorable energy deposition profile by the PFC damping. (b)The perpendicular gradient of E(+) squared is shown. The gradient is peaked at the plasma edge, indicating an unfavorable energy deposition profile by the DSH damping.

Fig. 12 The field patterns are shown for the first radial mode of the m=0 poloidal mode when the m=0 Fourier component of the antenna current equals one ampere. See the caption to Fig. 11 for explanations of the plotted quantities. The field pattern and energy deposition profile of this mode are more favorable than the mode in Fig. 11.

Fig. 13 The field patterns are shown for the tenth radial mode of the m=0 poloidal mode when the m=0 Fourier component of the antenna cureent equals one ampere. See the caption to Fig. 11 for explanations of the plotted quantities. The field pattern and energy deposition profile of this mode are highly favorable compared to those of modes in Fig. 11 and Fig. 12.

Fig. 14 Energetic proton tail distributions predicted by Stix's theory(16) for the Alcator-C and PLT. The on-axis densities of the Alcator-C is assumed to be 10 /m and of the PLT

2×10 /m . The lower and upper solid curves for the Alcator-C are for $T=T(i)=T(e)=1.0$ and 4.0 keV, respectively. The lower dotted curve for the PLT is for $T=1.0$ keV and rf power of 400 kW, and the upper curve for $T=4.0$ keV and 4 MW.

Fig. 15 The isometric drawing of the first Alcator-C antenna consisting of the antenna proper, return current strap and two protective limiters. The structure is made largely of stainless-steel and molybdenum. Some stainless-steel members are sublimated with a thin layer of molybdenum for better RF electrical conductivity.

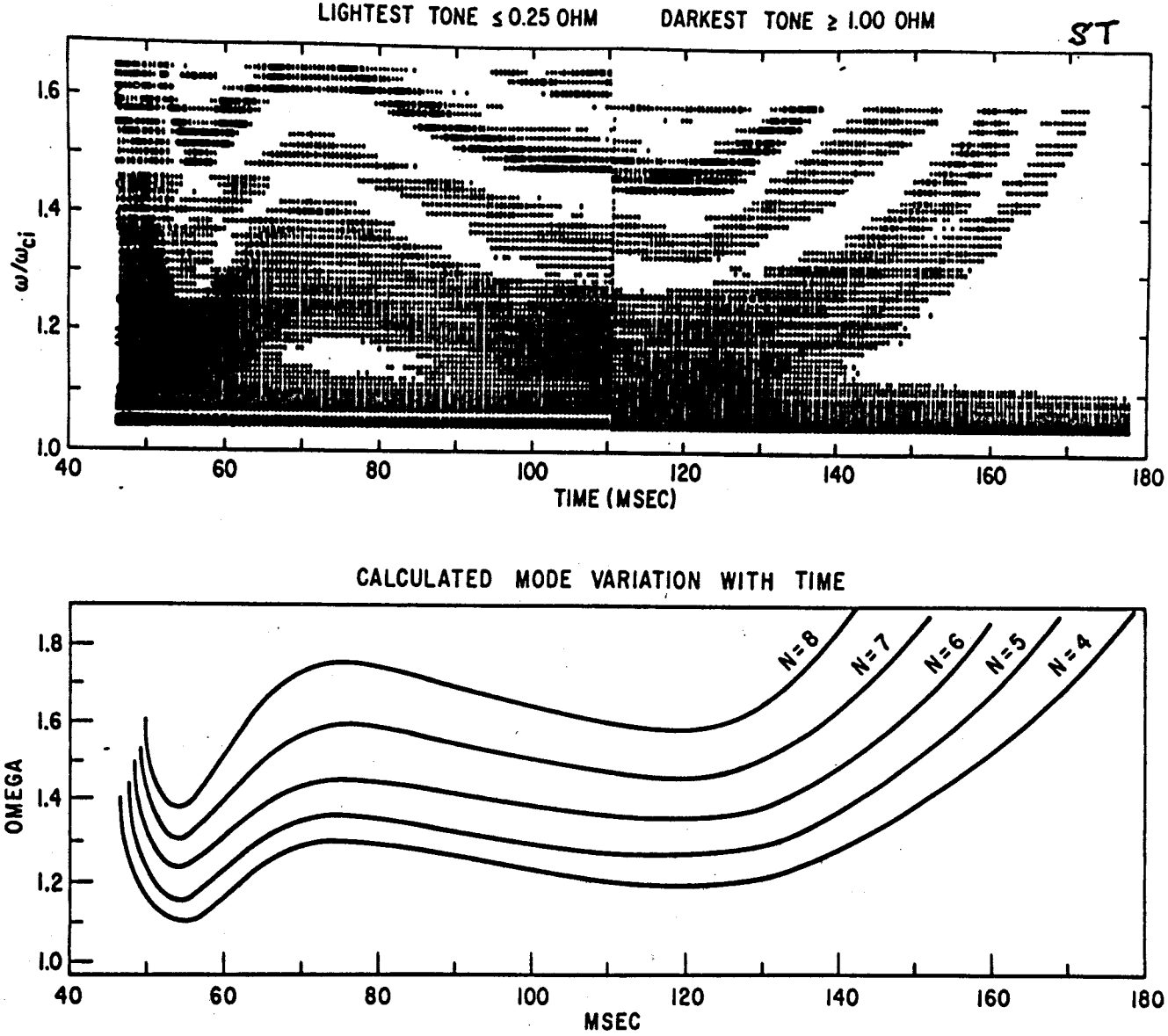
MEASURED SERIES LOADING RESISTANCE
LIGHTEST TONE ≤ 0.25 OHM
DARKEST TONE ≥ 1.00 OHM
ST
ω/ωci
1.0
1.2
1.4
1.6
40
60
80
100
120
140
160
180
TIME (MSEC)
CALCULATED MODE VARIATION WITH TIME
OMEGA
1.0
1.2
1.4
1.6
1.8
N=8
N=7
N=6
N=5
N=4
40
60
80
100
120
140
160
180
MSEC

Fig. 1

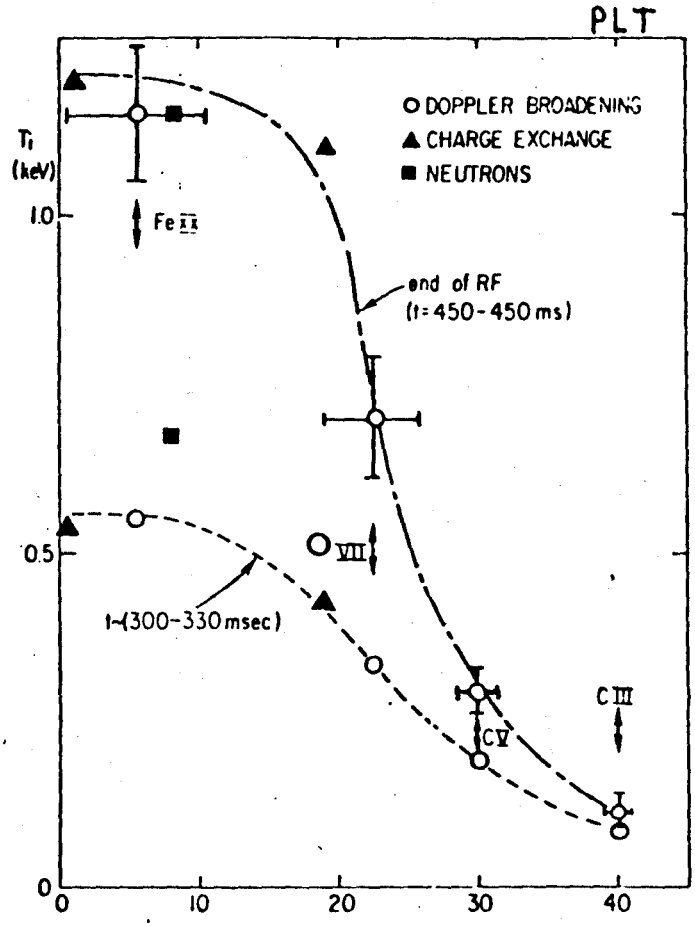
PLT
O DOPPLER BROADENING
▲ CHARGE EXCHANGE
■ NEUTRONS
T_i (keV)
1.0
0.5
0
Fe XX
end of RF
(t=450-450 ms)
O VII
t~(300-330 msec)
C III
C V
0
10
20
30
40

Fig. 2

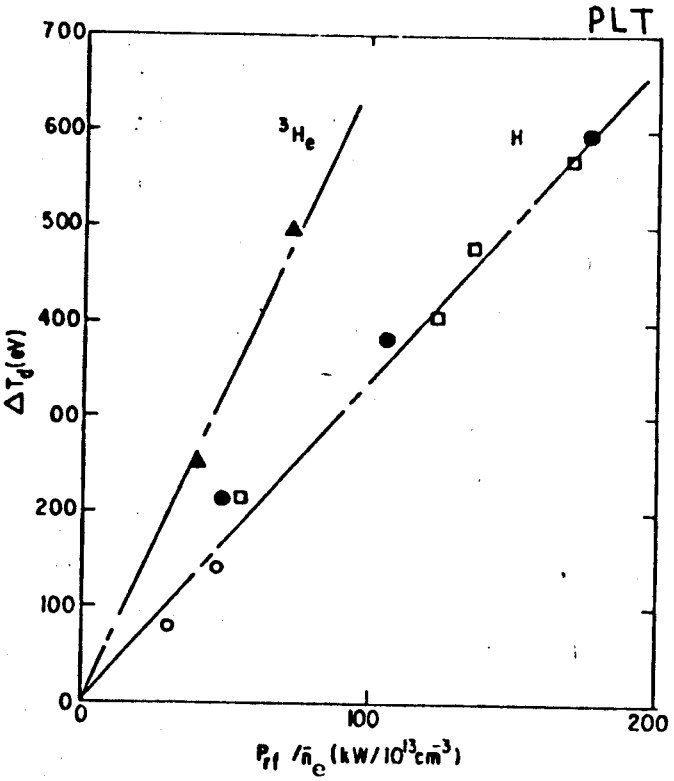
PLT
700
600
500
400
00
200
100
0
0
100
200
^3H_e
H
ΔT_e(eV)
$P_{rf}/\bar{n}_e$ (kW/10^{13}cm^{-3})

Fig. 3

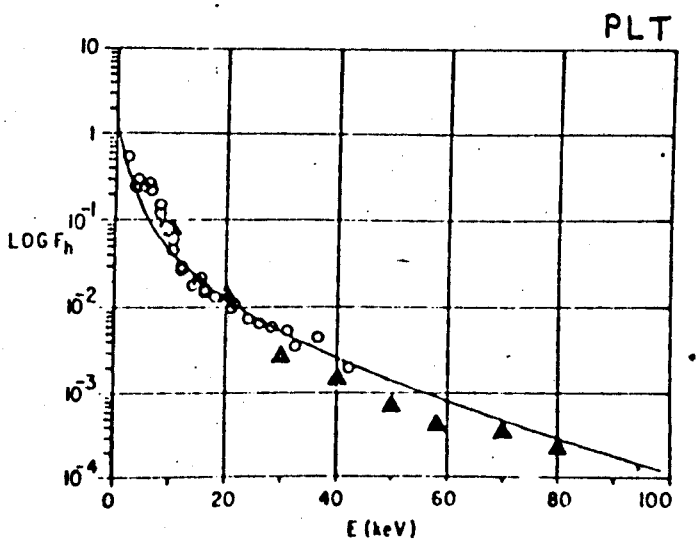

Fig. 4

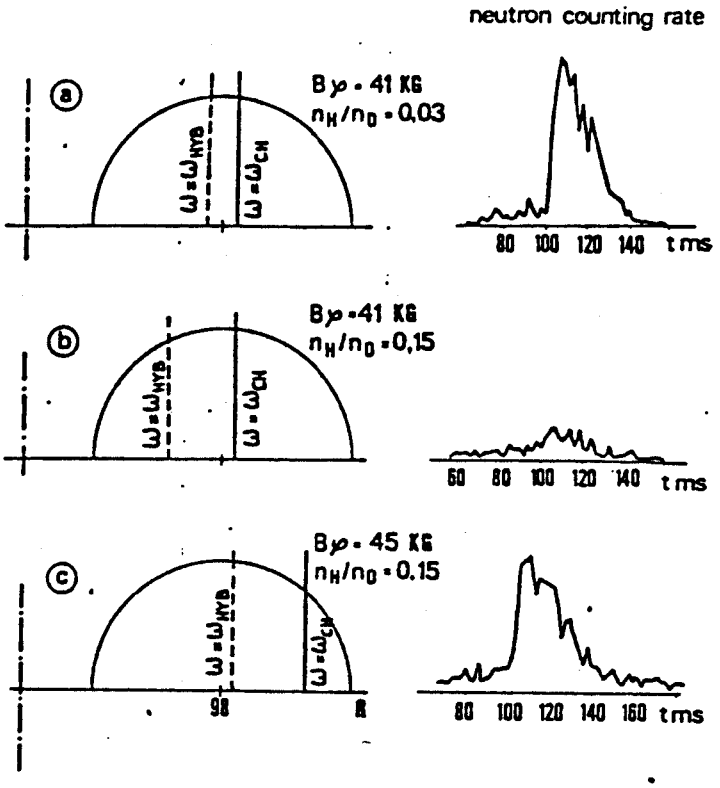
neutron counting rate
a
Bφ = 41 KG
n_H/n_D = 0.03
$\omega=\omega_{HYB}$
$\omega=\omega_{CH}$
80 100 120 140 t ms
b
Bφ = 41 KG
n_H/n_D = 0,15
$\omega=\omega_{HYB}$
$\omega=\omega_{CH}$
60 80 100 120 140 t ms
c
Bφ = 45 KG
n_H/n_D = 0.15
$\omega=\omega_{HYB}$
$\omega=\omega_{CH}$
98
R
80 100 120 140 160 t ms

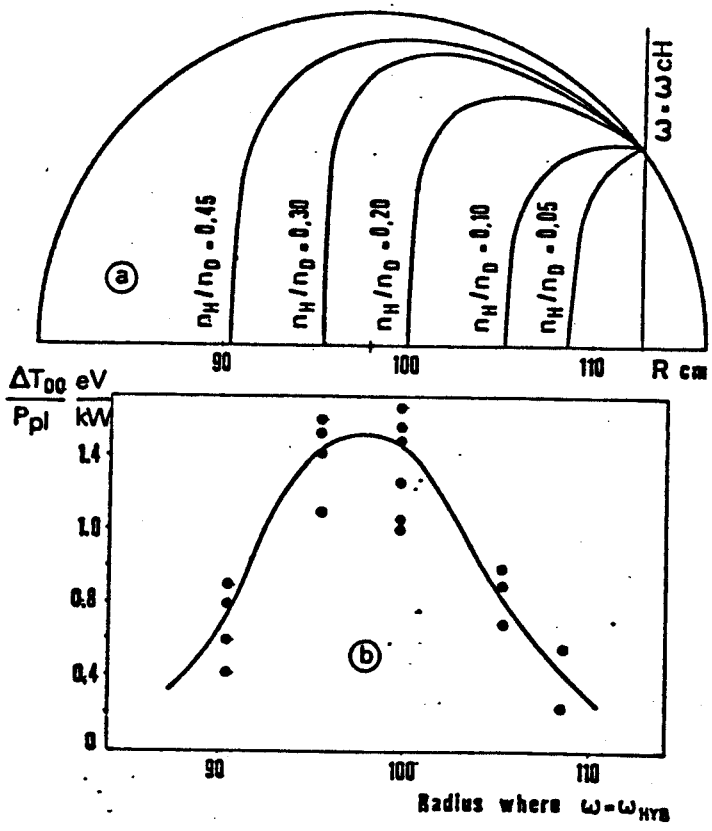
$\omega=\omega_{CH}$
a
n_H/n_D = 0,45
n_H/n_D = 0,30
n_H/n_D = 0,20
n_H/n_D = 0,10
n_H/n_D = 0,05
90
100
110
R cm
$\frac{\Delta T_{00}}{P_{pl}}$ eV/kW
1.4
1.0
0.8
0.4
0
b
90
100
110
Radius where $\omega=\omega_{HYB}$

TFR

Fig. 5

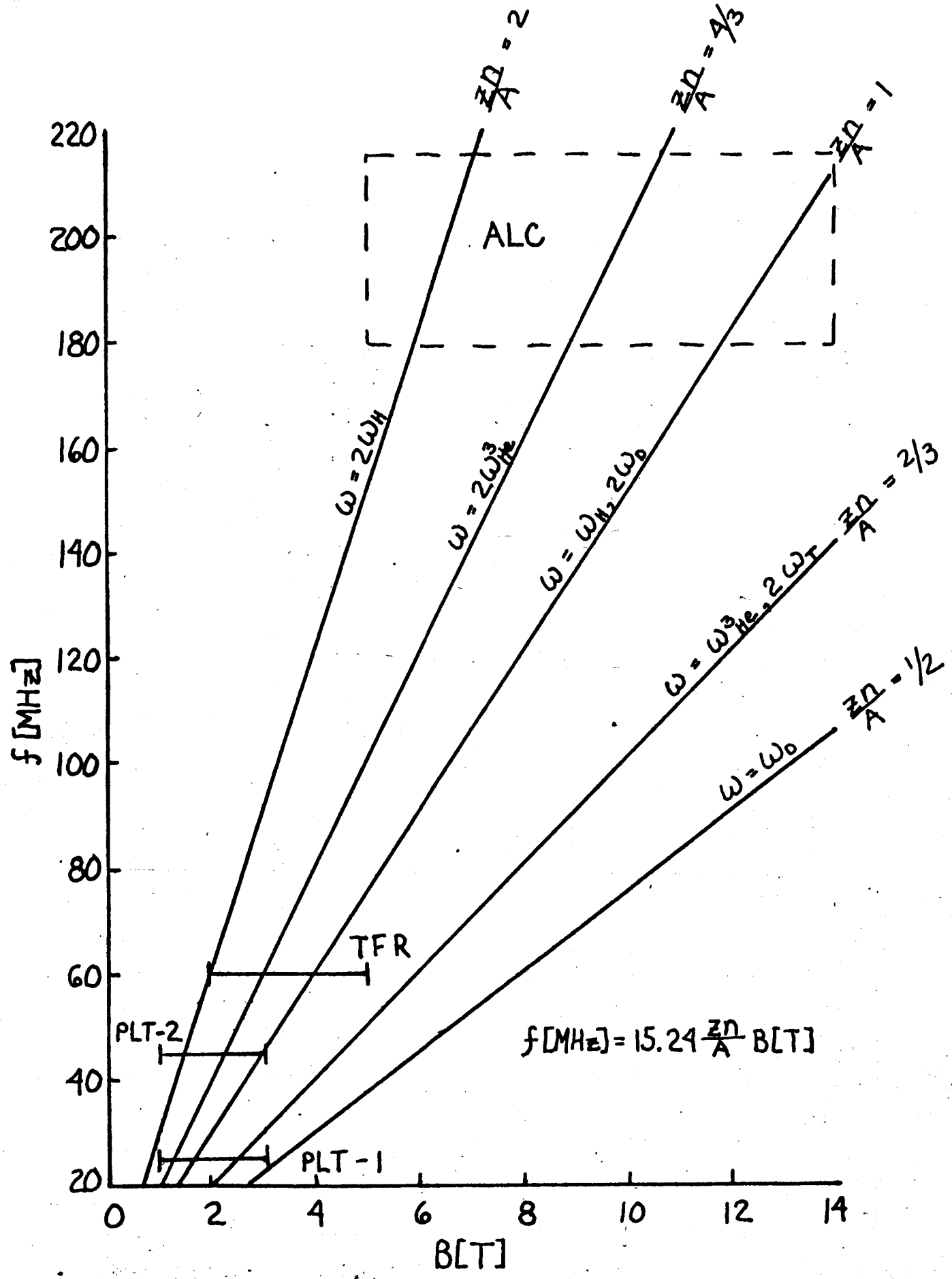
220
200
180
160
140
120
100
80
60
40
20
f [MHz]
0
2
4
6
8
10
12
14
B[T]
ALC
$\frac{zn}{A} = 2$
$\frac{zn}{A} = 4/3$
$\frac{zn}{A} = 1$
$\frac{zn}{A} = 2/3$
$\frac{zn}{A} = 1/2$
$\omega = 2\omega_H$
$\omega = 2\omega_{^3He}$
$\omega = \omega_H + 2\omega_D$
$\omega = \omega_{^3He} + 2\omega_T$
$\omega = \omega_D$
TFR
PLT-2
PLT-1
$f[MHz] = 15.24 \frac{zn}{A} B[T]$

Fig. 6

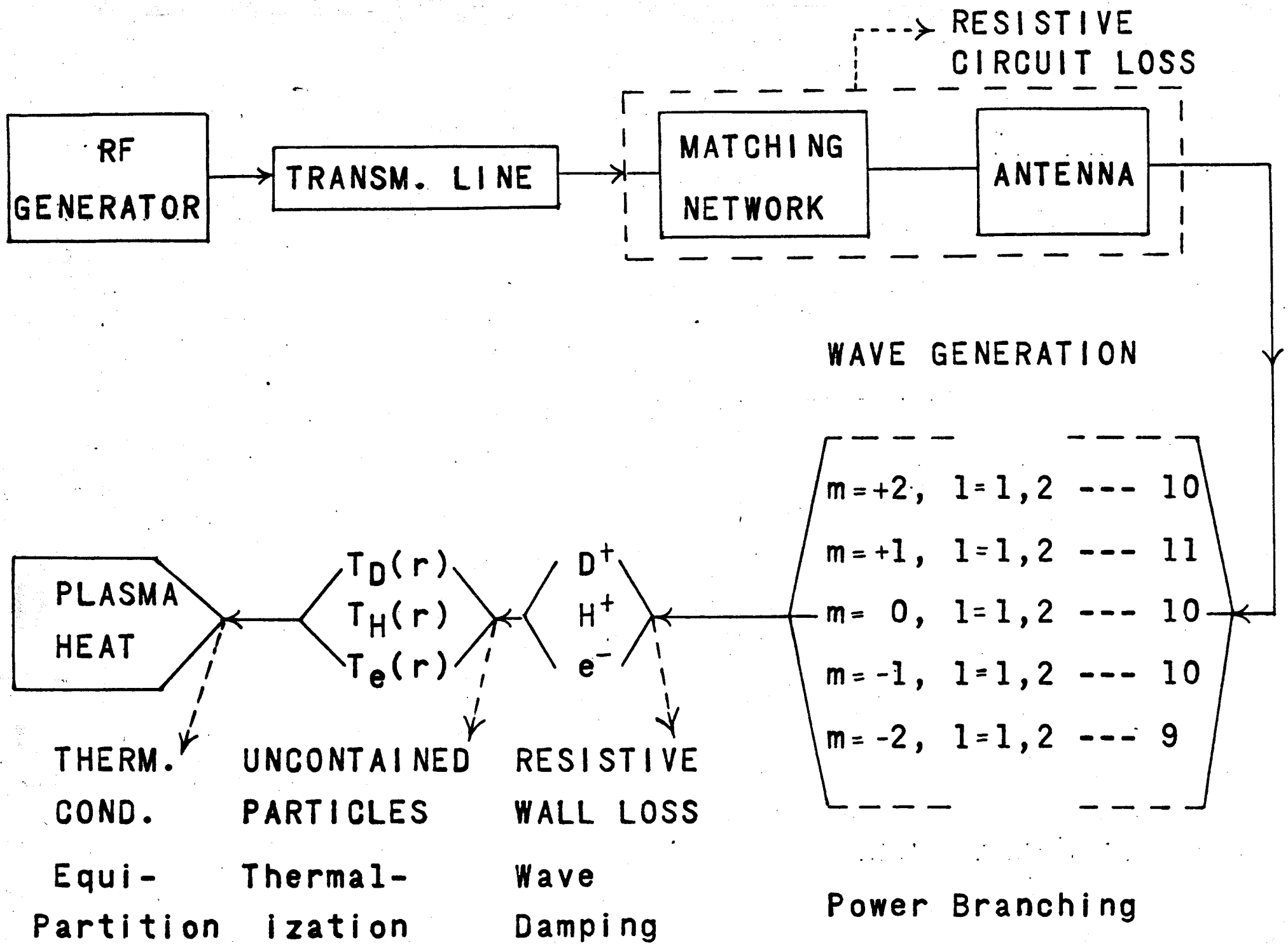
RESISTIVE
CIRCUIT LOSS
RF
GENERATOR
TRANSM. LINE
MATCHING
NETWORK
ANTENNA
WAVE GENERATION
m=+2, l=1,2 --- 10
m=+1, l=1,2 --- 11
m= 0, l=1,2 --- 10
m=-1, l=1,2 --- 10
m=-2, l=1,2 --- 9
Power Branching
PLASMA
HEAT
$T_D(r)$
$T_H(r)$
$T_e(r)$
D^+
H^+
e^-
THERM.
COND.
Equi-
Partition
UNCONTAINED
PARTICLES
Thermal-
ization
RESISTIVE
WALL LOSS
Wave
Damping

Fig. 7

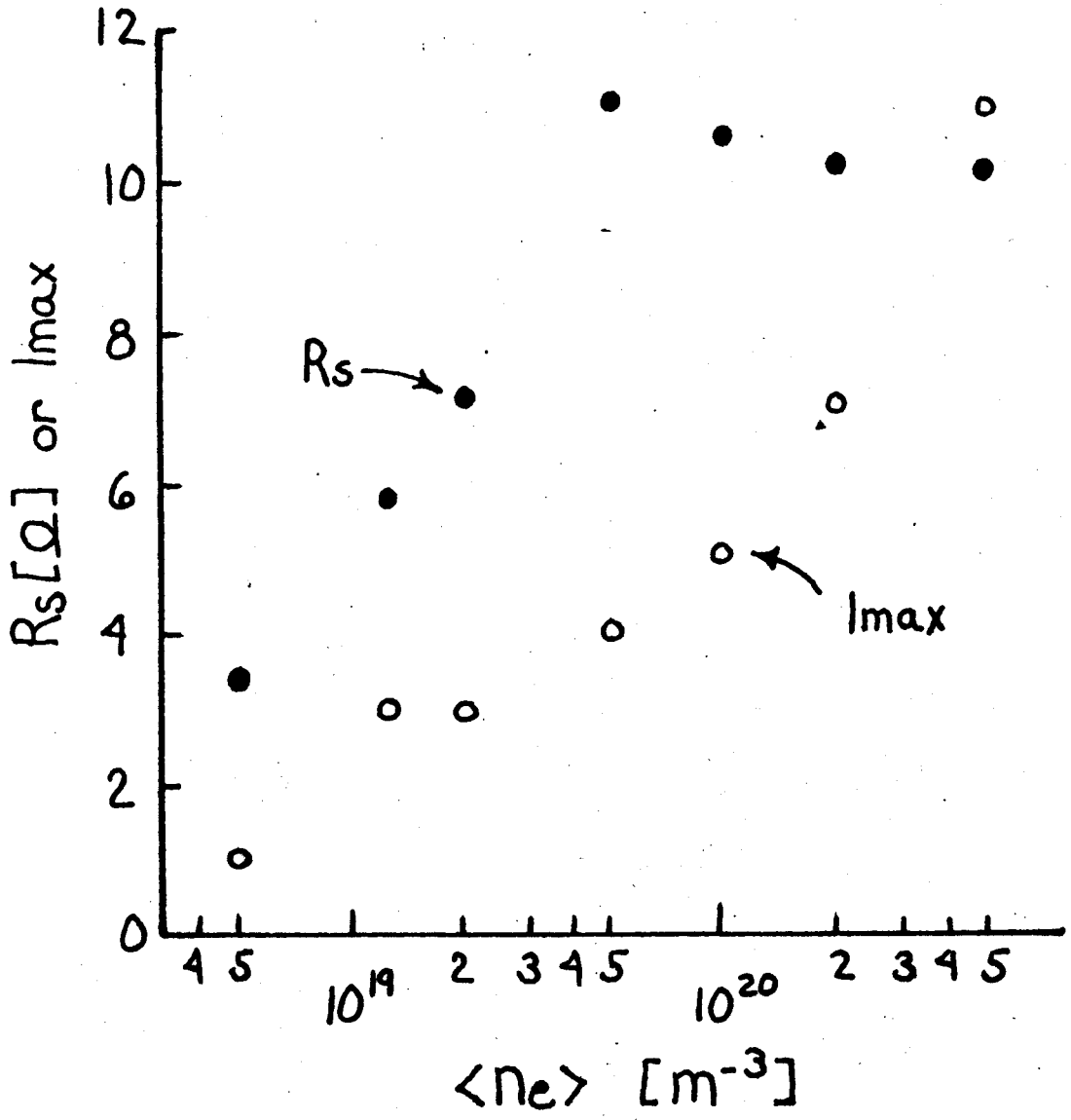

Fig. 8

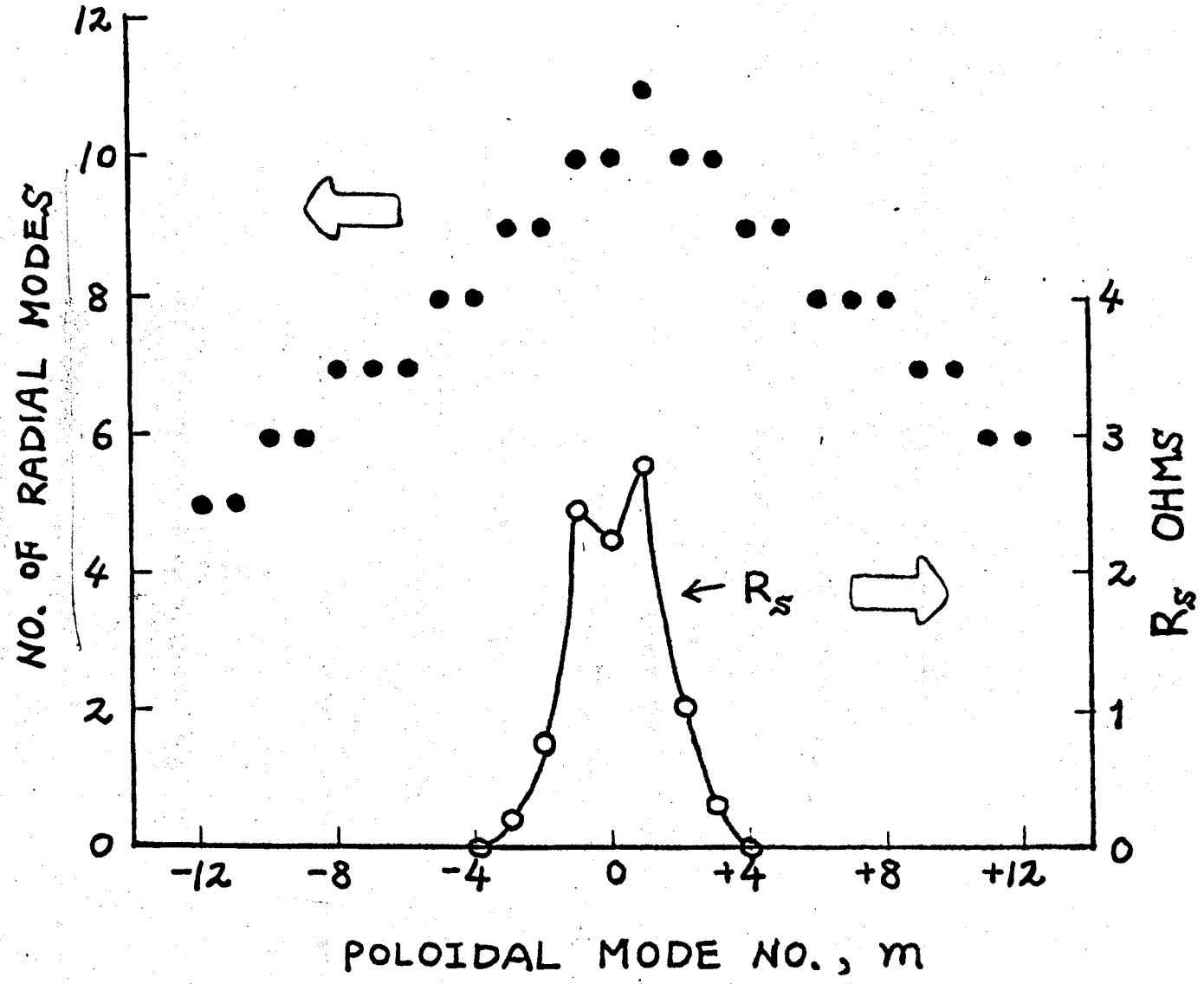
NO. OF RADIAL MODES
12
10
8
6
4
2
0
R_s
R_s OHMS
4
3
2
1
0
-12
-8
-4
0
+4
+8
+12
POLOIDAL MODE NO., m

Fig. 9

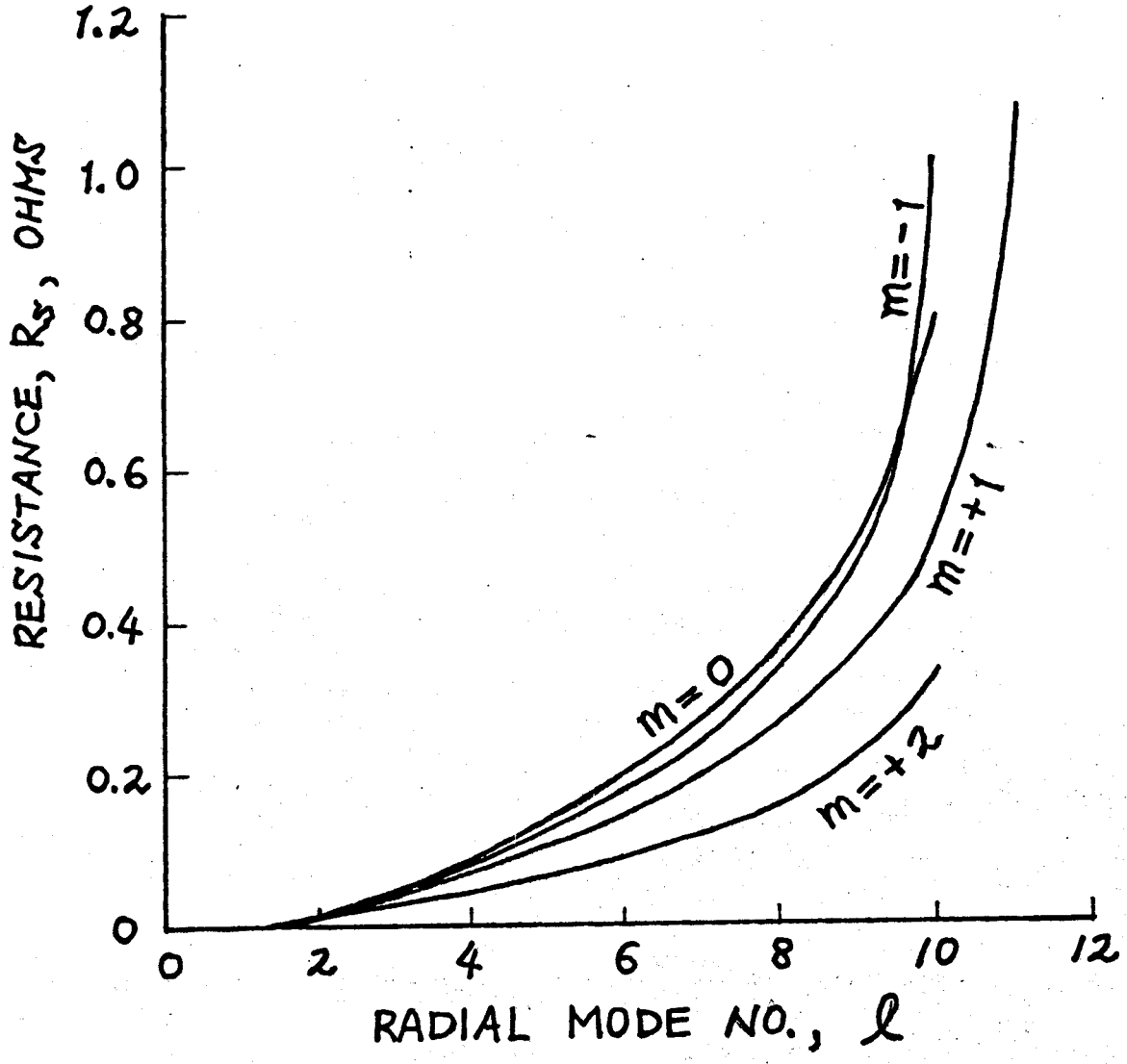
RESISTANCE, R_s, OHMS
1.2
1.0
0.8
0.6
0.4
0.2
0
0
2
4
6
8
10
12
RADIAL MODE NO., ℓ
m=-1
m=+1
m=0
m=+2

Fig. 10

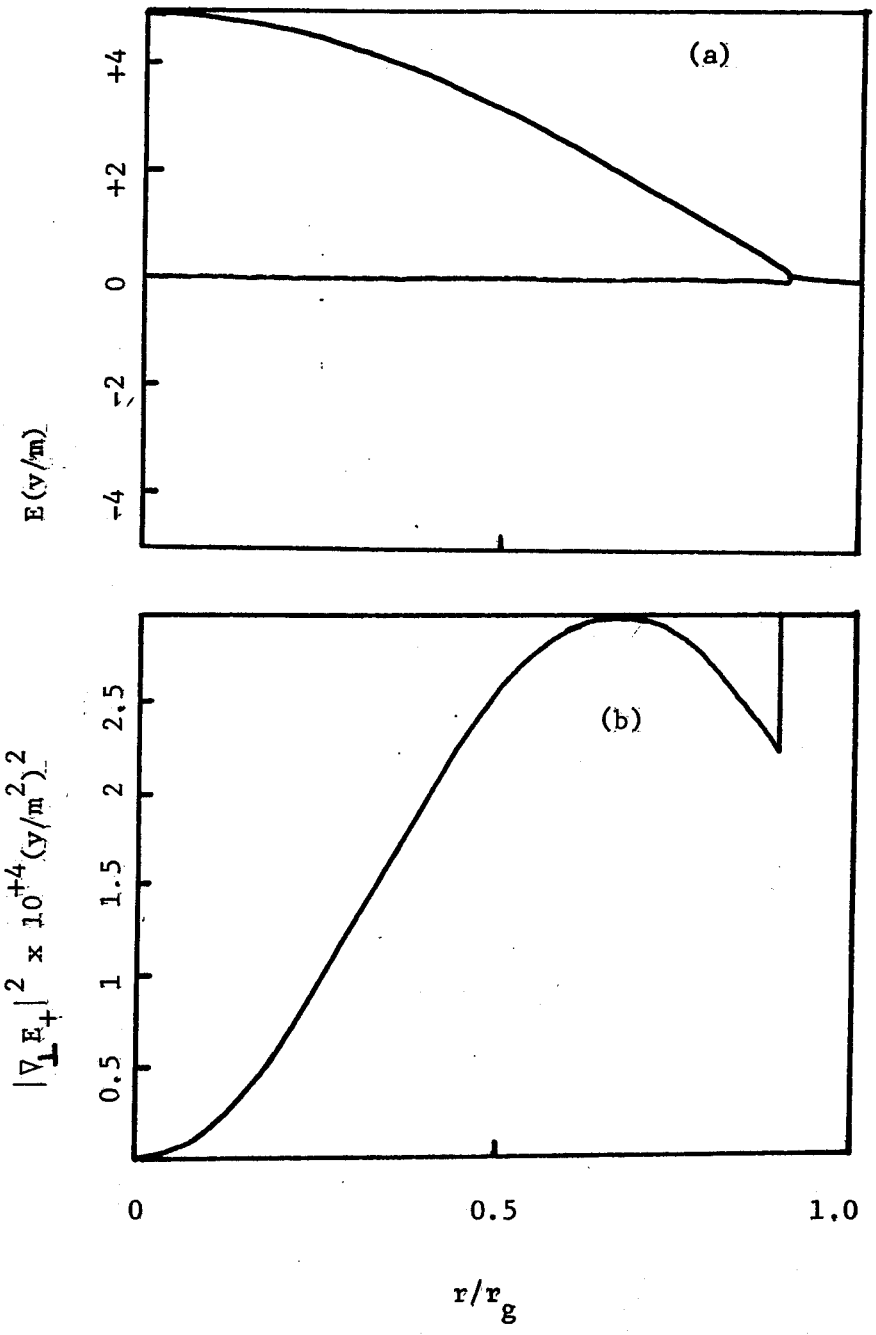

Fig. 11

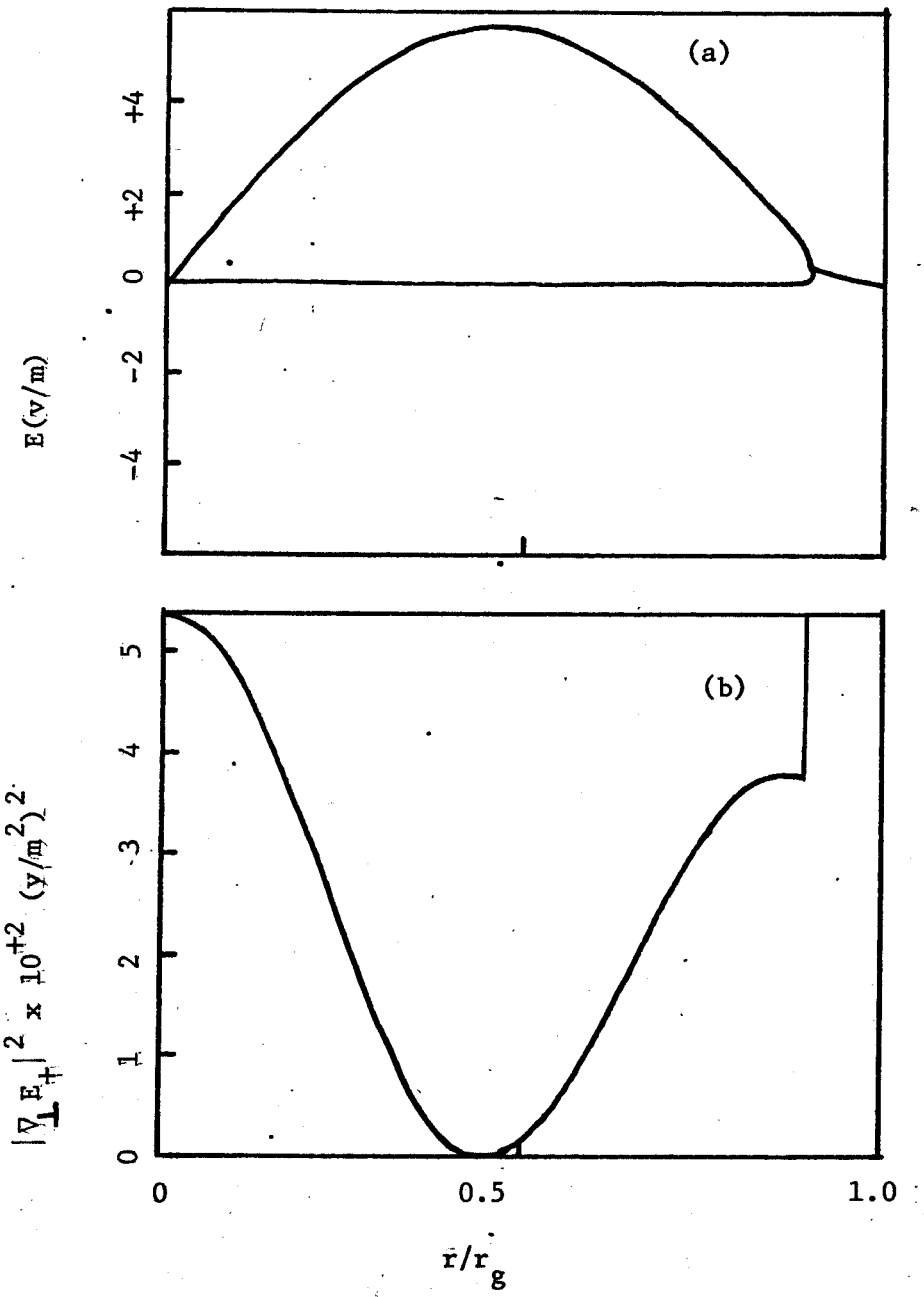

Fig. 12

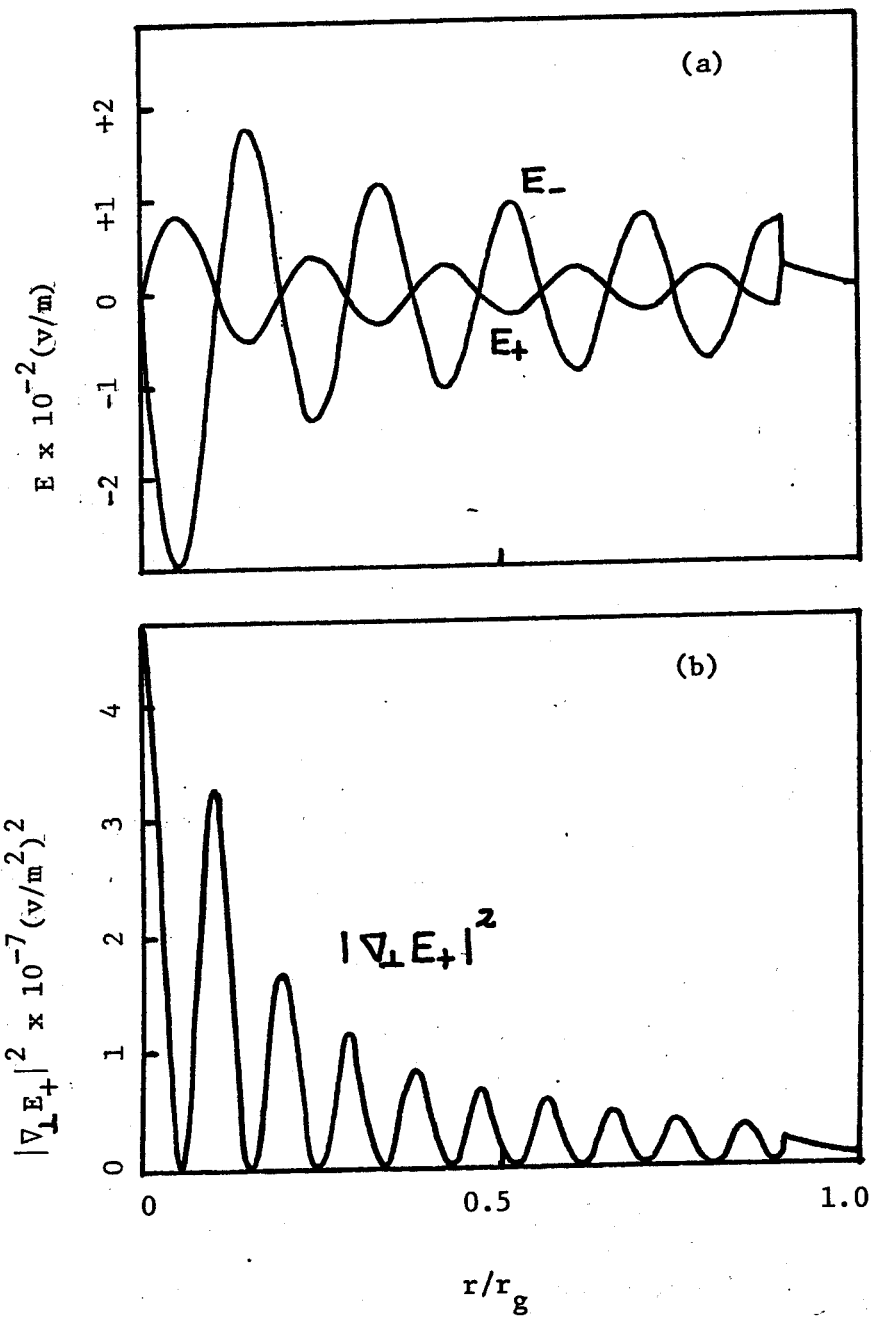

Fig. 13

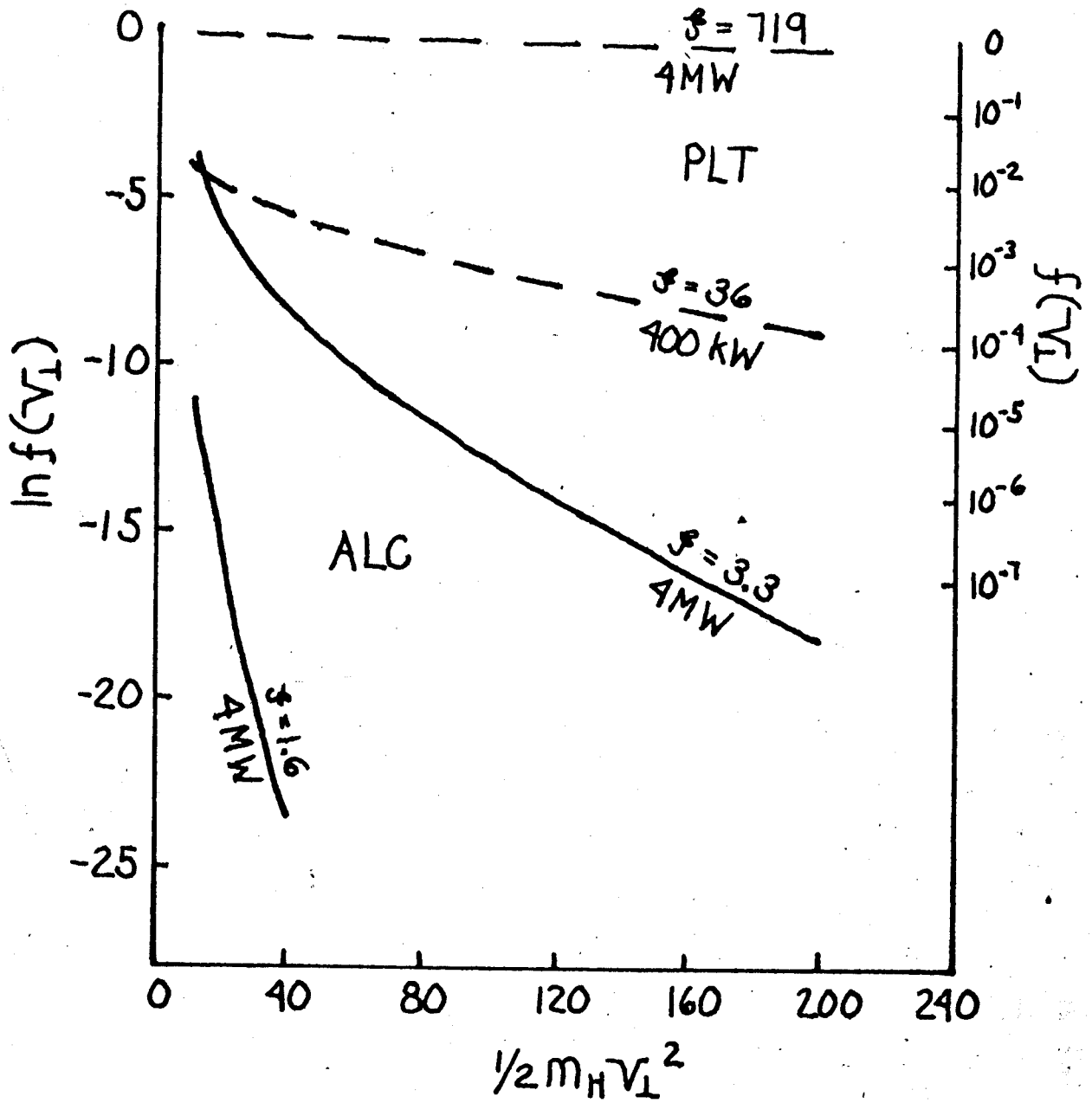
0
-5
-10
-15
-20
-25
ln f(V⊥)
0
40
80
120
160
200
240
½ m_H V⊥²
0
10⁻¹
10⁻²
10⁻³
10⁻⁴
10⁻⁵
10⁻⁶
10⁻⁷
f(V⊥)
β = 719
4MW
PLT
β = 36
400 kW
β = 3.3
4MW
ALC
β = 1.6
4MW

Fig. 14

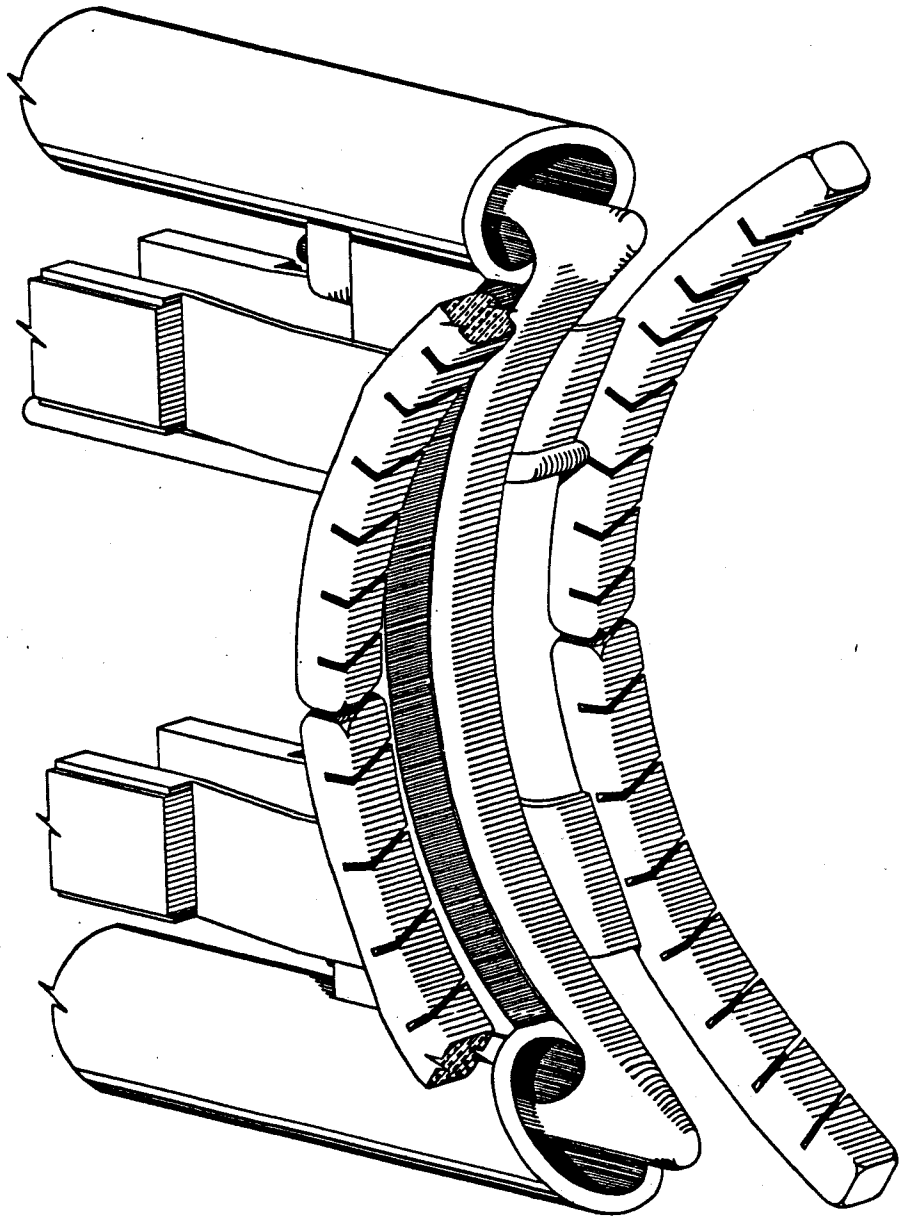

Fig. 15

ANTENNA ISOMETRIC
C 1599
D.NELSON OCT. 22,1979